frontiers | Frontiers in Earth Science

TYPE Original Research
PUBLISHED 21 February 2023
DOI 10.3389/feart.2023.1138170

OPEN ACCESS

EDITED BY
Yi-Xiang Chen,
University of Science and Technology of China, China

REVIEWED BY
Ren-Xu Chen,
University of Science and Technology of China, China
Songjie Wang,
Shandong University of Science and Technology, China
Tatsuki Tsujimori,
Tohoku University, Japan

*CORRESPONDENCE
Bin Xia,
xiabin@cug.edu.cn
Qin Yang,
yangqin@cug.edu.cn

SPECIALTY SECTION
This article was submitted to Petrology, a section of the journal Frontiers in Earth Science

RECEIVED 05 January 2023
ACCEPTED 13 February 2023
PUBLISHED 21 February 2023

CITATION
Lu X, Xia B, Yang Q and Wu Y (2023), Petrology and phase equilibria of HP/LT eclogite at Gaoqiao, western Dabie and implications for lawsonite development in continental subduction zones. *Front. Earth Sci.* 11:1138170. doi: 10.3389/feart.2023.1138170

Petrology and phase equilibria of HP/LT eclogite at Gaoqiao, western Dabie and implications for lawsonite development in continental subduction zones

Xianbin Lu, Bin Xia*, Qin Yang* and Yuanbao Wu

State Key Laboratory of Geological Processes and Mineral Resources, School of Earth Sciences, China University of Geosciences, Wuhan, China

Lawsonite is of great significance for understanding fluid activity, element migration and crust–mantle interactions in subduction zones. Though studies have predicted lawsonite to be present under the *P–T* regime during continental subduction, no lawsonite has been documented from natural (U) HP rocks in continental orogenic belt. In this study, we work on HP–LT eclogite (GQ–1 and GQ–2) at Gaoqiao, western Dabie to explore lawsonite formation and preservation during continental subduction and exhumation. Both samples have ubiquitous polymineralic aggregates of epidote/clinozoisite + paragonite/albite ± other minerals showing distinct rectangular or rhombic shapes developed as inclusions in garnet or in the matrix. Combined with recalculated bulk compositions similar to that of ideal lawsonite, we interpret these polymineralic aggregates to be pseudomorphs after lawsonite. Phase equilibrium modelling combined with compositional isopleth thermobarometry have constrained a segment of the prograde to peak stages to evolve from 19.0 to 19.5 kbar, ~470°C to ~20.0 kbar, 500C–505°C, then to ~25 kbar, 530C–555°C in lawsonite stability fields. The prograde *P–T* path shows a two-stage *P–T* evolution, with the first stage following a geothermal gradient of ~7°C/km and the second stage decreasing to ~6°C/km. Initial exhumation was inferred to follow an isothermal decompression process leading to lawsonite breakdown to form epidote/clinozosite ± paragonite *via* the reaction lawsonite + omphacite→ epidote + glaucophane ± paragonite + H_2O at ~19 kbar, 550°C. Modeled *P/T–X* pseudosections calculated at T = 550°C and p = 25 kbar show that, when H_2O content in bulk composition is more than 1.1 wt%, a certain amount of lawsonite (>13 mode%) should be present in eclogite. On the other hand, in the compositional range of natural intracontinental plate basalts, variations on O (Fe^{3+}), X_{MgO} [MgO/(MgO+FeO)], X_{CaO} [CaO/(CaO+MgO+FeO+MnO+Na_2O)], X_{Na2O} [(Na_2O/(CaO+Na_2O)] and X_{Al2O3} [Al_2O_3/(Al_2O_3+CaO+Na_2O)] in bulk compositions have little influence on lawsonite development. In combination with previous studies, we conclude that during continent subduction along low geothermal gradient (<8°C/km), lawsonite could be formed under H_2O present conditions. The absence of lawsonite in natural eclogite might be ascribed to retrograde overprint during exhumation.

KEYWORDS

lawsonite, eclogite, phase equilibrium modeling, continental subduction zone, western Dabie

1 Introduction

Fluid activities in subduction zones are essential in understanding arc magmatism, crustal-mantle material circulation, mineralization and earthquakes (Tatsumi, 1989; Scambelluri and Philippot, 2001; Miller et al., 2002; Schmidt and Poli, 2003; Tatsumi and Kogiso, 2003; Zheng, 2009; Zheng et al., 2011; Zheng, 2012). Lawsonite is a significant H_2O-carrier mineral with water content up to 11.5 wt% (Spandler et al., 2003; Reynard and Bass, 2014; Tsujimori and Ernst, 2014; Vitale Brovarone et al., 2014), also a significant LREE-, Sr-, Pb-carrier minerals (Spandler et al., 2003; Martin et al., 2014; Hara et al., 2018). Experimental studies show that lawsonite could be formed under low-temperature and high-pressure conditions and may convey great amount water into great depths (>200 km) in subduction zones (Poli and Schmidt, 1995; Okamoto and Maruyama, 1999). Therefore, lawsonite is one of the most important minerals for the study of fluid activities in subduction zones. In natural rocks, lawsonite is commonly developed in (U)HP/LT metamorphic rocks from ancient oceanic subduction orogenic belts (Okamoto and Maruyama, 1999; Whitney and Davis, 2006), with only rarely been reported from eclogite xenoliths in kimberlite (Smith and Zientek, 1979; Usui et al., 2006). However, in continental orogenic belts, although petrographic studies, geochemistry and phase equilibrium modelling have predicted the existence of lawsonite under fluid-present conditions in (U)HP/LT environment, no lawsonite grain has been reported yet (Li et al., 2004; 2005; Angiboust and Agard, 2010; Wei, 2011; Guo et al., 2013; Orozbaev et al., 2015; Ren et al., 2018). Besides, factors controlling the formation and stability of lawsonite that dictate the fluid availability during continental subduction are still controversial (Tsujimori et al., 2006; Wei, 2011; Hamelin et al., 2018; Ren et al., 2018).

The Sulu–Dabie mountain is a classic continental subduction-collisional orogenic belt formed by the Triassic collision between the south China Block and the north China Block (Zheng, 2008; Wu et al., 2009; Wu and Zheng, 2013). In the western Dabie, well-preserved HP/UHP metamorphic rocks have peak *P–T* conditions of 26–31 kbar and 520°C–670°C (Liu et al., 2004a; Liu et al., 2006; Wei et al., 2010; Xia et al., 2022a; b), locating in lawsonite-eclogite facies fields. Besides, ubiquitous veins in eclogites and their host rocks manifest presence of fluid during eclogite facies metamorphism (Liu et al., 2004a; Cheng et al., 2009; Wei et al., 2010), beneficial for the formation of lawsonite. In this study, we show eclogites at Gaoqiao, western Dabie have abundant composite mineral aggregates of epidote/clinozoisite + paragonite/albite ± other minerals with distinct rectangular or rhombic shapes in the matrix or as inclusions in garnet. These polymineralic aggregates were demonstrated to be pseudomorphs after lawsonite. To establish the *P–T* evolution and explore factors influencing the development and decomposition of lawsonite during continental subduction and exhumation, we performed detailed petrography, mineral chemistry and phase equilibrium modeling on eclogites at Gaoqiao, western Dabie. Mineral abbreviations in this study follow those used by the thermodynamic dataset of Holland and Powell (1998).

2 Geological setting

Geologically, western Dabie is separated from the Tongbai orogen by Dawu Fault to the west and from eastern Dabie orogen by Shangma Fault to the east (Figures 1A, B). Previous studies have shown that western Dabie is a huge antiform with UHP rocks at the core and HP rocks at the two limbs (Hacker et al., 2000; Liu et al., 2004a; Wu et al., 2008). Lithologies in western Dabie are mainly metasedimentary rocks and granitic gneisses, and minor eclogites, blueschists, greenschists as blocks, lenses and intercalated layers within them (Liu et al., 2004a). From south to north, based on litho-tectonic features and metamorphic grades, six units can be subdivided (Figure 1B): the Mulanshan blueschist–greenschist unit, the Hong'an HP eclogite unit, the Xinxian UHP eclogite unit, the Huwan HP eclogite unit, the Baliban tectonic mélange unit and the Nanwan flysch unit (Zhong et al., 1999; 2001; Liu et al., 2004a; b). Previous studies have shown that, P_{max}–T conditions for metamorphic rocks at Mulanshan are 8–11 kbar, 320C–430°C (Liu et al., 2004a), at Hong'an are 19–26 kbar, 485°C–585°C (Liu et al., 2004a; Cheng et al., 2010; Lou et al., 2013), at Xinxian are 28–32 kbar, 520C–670°C (Zhang and Liou, 1994; Liu et al., 2004a; Liu et al., 2006; Wei et al., 2010; Xia et al., 2022a), at Huwan are 18–23 kbar, 540°C–630°C (Liu et al., 2004a; Ratschbacher et al., 2006; Zhou et al., 2014; 2015; Cheng and Cao, 2015) and at Balifan are 9–10 kbar, 460°C–515°C (Liu et al., 2004a).

A larger number of geochronological studies on blueschist, eclogite and the host granitic gneisses and metasedimentary rocks have conformed the consistency on eclogite facies metamorphism in western Dabie and the eastern Dabie and Sulu belts, which constitute a huge continuous Triassic orogenic belt. For instance, in western Dabie, the prograde stage metamorphism was constrained to be 239–226 Ma, the peak UHP metamorphism to be ~226 Ma, the early retrograde eclogite facies metamorphism to be 216–213 Ma and the later retrograde amphibolite facies metamorphism to be ~212 Ma (Wu and Zheng, 2013 and references therein). However, in Huwan shear zone, late Carboniferous eclogite facies metamorphism ages of ~310 Ma have been reported for eclogite and its country rock gneisses (Wu et al., 2009; Liu et al., 2011). In combination with some eclogites showing oceanic crust geochemical signatures, the eclogite facies metamorphism was interpreted to represent an early oceanic subduction (Wu and Zheng, 2013; Zhou et al., 2015).

3 Samling and analytical methods

3.1 Sampling

In this study, eclogite samples were collected at Gaoqiao in the Hong'an HP eclogite unit, western Dabie (Figure 1B). Eclogites at Gaoqiao occur either as blocks (4–8 m in diameter) or as intercalated layers (0.5–4 m in width) in the host garnet micaschist (Figure 1C). Various types of veins, including phengite–quartz veins and quartz–epidote–calcite veins developed in eclogites (Figure 1D). At some places, elongated eclogite fragments are found in micaschist, with quartz veins roughly along schistosity in the host rock (Figures 1E, F). To quantify *P–T* evolution for eclogite at Gaoqiao, we select two eclogite samples (GQ–1 and GQ–2)

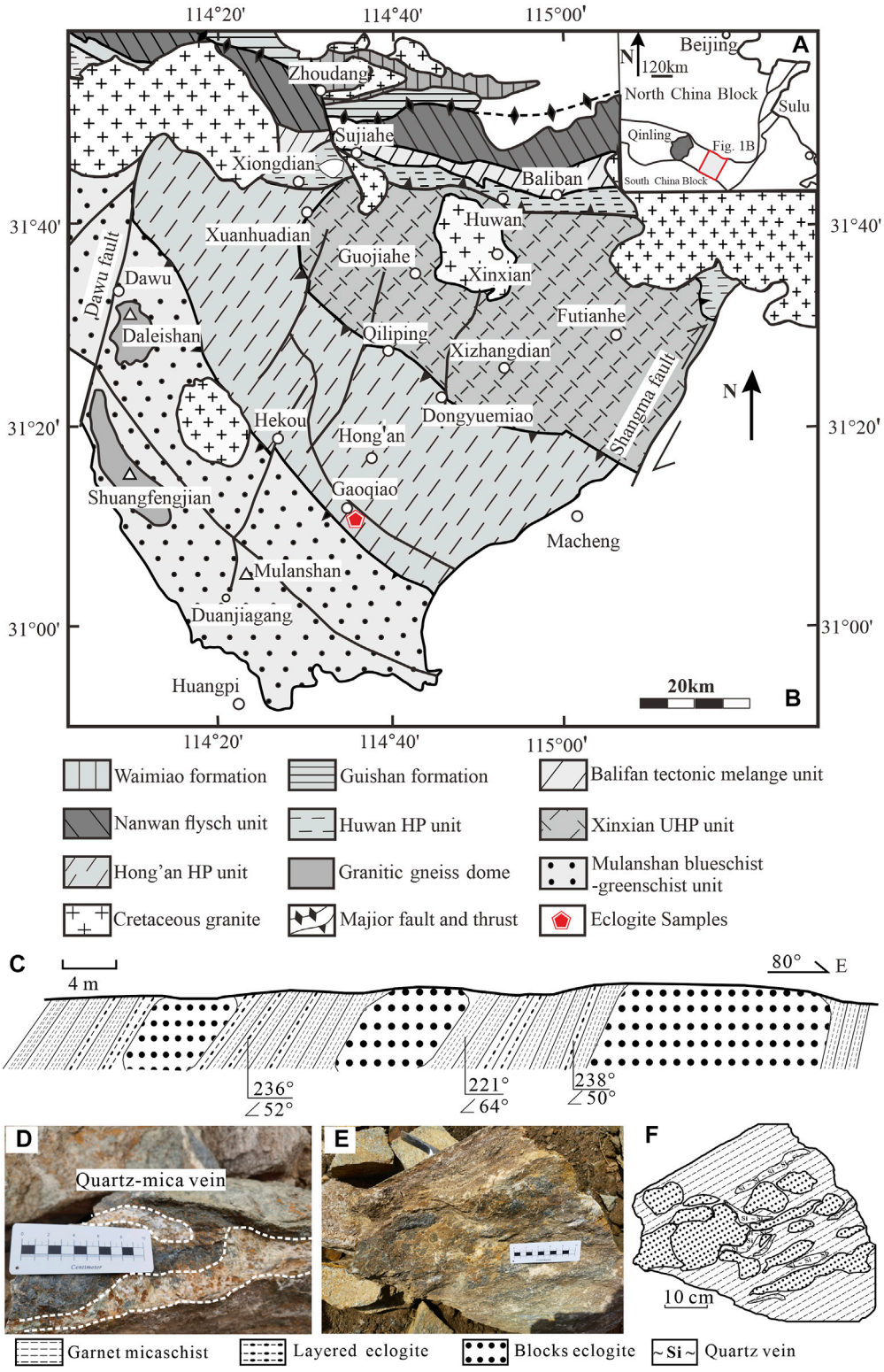

FIGURE 1
(A) Tectonic framework of the Sulu-Dabie-Qingling orogen in central China. **(B)** Simplified geological map of western Dabie (modified after Liu et al., 2004a). In this study, eclogite was sampled at Gaoqiao in the Hong'an HP eclogite unit, western Dabie. **(C)** Cross-section of eclogite and country rock at Gaoqiao, western Dabie. Eclogite occurs as blocks (4–8 m in diameter) or intercalated layers (0.5–4 m in width) in the country rock garnet micaschist. **(D)** Quartz-muscovite veins developed in layered eclogite. **(E)** Elongated eclogite fragments and quartz veins roughly along schistosity in micaschist. **(F)** Sketch of field features for **(E)**.

TABLE 1 Representative compositions of garnet, paragonite and phengite from eclogite at Gaoqiao, western Dabie.

Mineral Position	GQ-1	GQ-1	GQ-1	GQ-1	GQ-1	GQ-1	GQ-1	GQ-1	GQ-2	GQ-2	GQ-2	GQ-2	GQ-2	GQ-2	GQ-2	GQ-2
	g	g	g	g	ph	ph	pa	pa	g	g	g	g	ph	ph	pa	pa
	c	m	m	r	in g	matrix	in g	matrix	c	m	m	r	in g	matrix	in g	matrix
SiO_2	37.78	37.64	37.87	38.03	52.63	49.55	47.647	46.14	37.95	37.83	37.84	38.07	53.15	49.74	48.37	48.40
TiO_2	0.08	0.14	0.20	0.03	0.15	0.22	0.06	0.07	0.12	0.17	0.18	0.07	0.12	0.21	0.02	0.02
Al_2O_3	21.13	21.03	21.15	21.82	28.61	30.69	40.23	38.25	21.18	21.15	21.39	21.55	24.73	28.89	38.91	39.59
Cr_2O_3	0.05	0.02	0.03	0.00	0.02	0.04	0.02	0.05	0.00	0.01	0.00	0.00	0.00	0.01	0.00	0.00
FeO	22.67	26.67	27.51	29.12	1.43	2.07	0.38	0.23	22.59	26.86	28.06	29.16	1.90	2.82	0.80	0.30
MnO	6.46	2.09	0.84	0.10	0.02	0.00	0.02	0.00	6.48	1.56	0.68	0.13	0.00	0.02	0.03	0.00
MgO	0.80	1.07	1.37	3.38	3.48	3.17	0.11	0.25	0.87	1.17	1.32	3.25	4.44	2.96	0.15	0.12
CaO	11.47	11.12	11.31	8.00	0.00	0.03	0.18	0.19	11.31	11.36	11.71	8.15	0.00	0.02	0.18	0.16
Na_2O	0.04	0.05	0.00	0.01	0.72	0.85	6.29	6.99	0.01	0.04	0.01	0.00	0.32	0.57	5.60	6.84
K_2O	0.00	0.01	0.00	0.00	9.51	7.51	0.67	0.54	0.00	0.01	0.00	0.00	10.66	10.19	0.73	0.47
Total	100.48	99.84	100.29	100.48	96.56	94.14	95.61	92.72	100.51	100.14	101.19	100.39	95.32	95.44	94.79	95.90
O	12.00	12.00	12.00	12.00	11.00	11.00	11.00	11.00	12.00	12.00	12.00	12.00	11.00	11.00	11.00	11.00
Si	3.00	3.00	3.00	2.99	3.42	3.27	3.01	3.02	3.01	3.01	2.98	3.00	3.53	3.32	3.08	3.05
Ti	0.01	0.01	0.01	0.00	0.01	0.01	0.00	0.00	0.01	0.01	0.01	0.00	0.01	0.01	0.00	0.00
Al	1.98	1.98	1.98	2.02	2.19	2.39	3.00	2.95	1.98	1.98	1.98	2.00	1.94	2.27	2.92	2.94
Cr	0.00	0.00	0.00	0.00	0.00	0.00	0.00	0.00	0.00	0.00	0.00	0.00	0.00	0.00	0.00	0.00
Fe^{3+}	0.02	0.00	0.00	0.00	0.00	0.08	0.01	0.00	0.00	0.00	0.05	0.00	0.00	0.03	0.03	0.00
Fe^{2+}	1.49	1.78	1.82	1.91	0.08	0.03	0.01	0.01	1.50	1.78	1.80	1.92	0.11	0.13	0.01	0.02
Mn	0.43	0.14	0.06	0.01	0.00	0.00	0.00	0.00	0.44	0.11	0.05	0.01	0.00	0.00	0.00	0.00
Mg	0.10	0.13	0.16	0.40	0.34	0.31	0.01	0.03	0.10	0.14	0.16	0.38	0.44	0.29	0.01	0.01
Ca	0.98	0.95	0.96	0.67	0.00	0.00	0.01	0.01	0.96	0.97	0.99	0.69	0.00	0.00	0.01	0.01
Na	0.01	0.01	0.00	0.00	0.09	0.11	0.77	0.89	0.00	0.01	0.00	0.00	0.04	0.07	0.69	0.84
K	0.00	0.00	0.00	0.00	0.79	0.63	0.05	0.05	0.00	0.00	0.00	0.00	0.90	0.87	0.06	0.04
Sum	8.00	8.00	8.00	8.00	6.91	6.85	6.89	6.96	8.00	8.00	8.00	8.00	6.97	6.99	6.82	6.91
alm	0.50	0.59	0.61	0.64					0.50	0.60	0.60	0.64				
spss	0.15	0.05	0.02	0.00					0.15	0.04	0.02	0.00				
py	0.03	0.04	0.05	0.13					0.03	0.05	0.05	0.13				
gr	0.33	0.32	0.32	0.23					0.32	0.32	0.33	0.23				

Note: c, core; m, mantle; r, rim. In g, as inclusions in garnet; matrix, as rock–forming minerals in the matrix.

from the intercalated layers for petrology and phase equilibrium modeling.

3.2 Analytical methods

The major-element compositions of the minerals were analyzed using a JEOL JXA-8100 electron probe microanalyzer (EPMA) at the Key Laboratory of Submarine Geosciences, Second Institute of Oceanography, Ministry of Natural Administration, and the JEOL JXA-8230 EPMA at the Center for Global Tectonics, School of Earth Sciences, China University of Geosciences (Wuhan), respectively. During the experimental operation, the acceleration voltage is set to 15 kV, the current is 20 nA, and the beam spot diameter is 1 or 5 μm. Dwell times were 10 s on element peaks and half that on background locations adjacent to peaks. Raw X-ray intensities were corrected using a ZAF (atomic number, absorption, fluorescence) correction procedure. A series of natural and synthetic SPI standards were

TABLE 2 Representative compositions of omphacite, amphibole albite and epidote from eclogite at Gaoqiao, western Dabie.

Mineral Position	GQ-1	GQ-1	GQ-1	GQ-1	GQ-1	GQ-1	GQ-1	GQ-1	GQ-1	GQ-2	GQ-2	GQ-2	GQ-2	GQ-2	GQ-2	GQ-2
	o	o	amp	amp	gl	gl	ep	ep	ab	o	o	amp	amp	ep	ep	ab
	in g	matrix	in g	matrix	matrix	matrix	in g	in g	in g	in g	matrix	in g	matrix	in g	in g	in g
SiO_2	54.97	55.50	43.68	49.36	58.17	58.97	39.09	37.85	67.56	55.11	55.40	47.03	46.60	38.63	37.46	67.49
TiO_2	0.00	0.01	0.19	0.07	0.00	0.02	0.25	0.08	0.00	0.00	0.04	0.26	0.29	0.16	0.11	0.00
Al_2O_3	9.87	12.27	14.77	11.36	12.62	12.12	30.60	26.90	19.18	10.03	11.64	10.66	13.69	29.62	22.20	19.91
Cr_2O_3	0.08	0.01	0.00	0.00	0.00	0.00	0.00	0.04	0.00	0.05	0.02	0.00	0.07	0.01	0.01	0.00
FeO	6.06	4.73	21.53	12.51	7.89	8.02	2.16	7.05	0.39	5.79	3.81	16.44	11.22	4.22	13.31	0.17
MnO	0.16	0.00	0.01	0.00	0.00	0.00	0.01	0.16	0.06	0.01	0.01	0.00	0.04	0.05	0.05	0.00
MgO	7.72	6.83	5.58	12.14	10.98	11.16	0.14	0.01	0.01	7.78	7.54	9.90	12.04	0.14	0.02	0.01
CaO	13.38	11.69	8.00	8.23	0.77	0.40	24.23	23.27	0.12	13.93	12.54	8.55	8.19	23.44	22.70	0.28
Na_2O	6.99	7.38	4.16	3.79	6.83	6.89	0.00	0.00	11.73	6.38	7.08	3.64	4.54	0.04	0.03	11.80
K_2O	0.00	0.01	0.04	0.22	0.00	0.02	0.00	0.01	0.02	0.00	0.00	0.26	0.42	0.16	0.01	0.01
Total	99.23	98.42	97.96	97.68	97.27	97.61	96.48	95.35	99.08	99.06	98.06	96.74	97.08	96.47	96.19	99.67
O	6.00	6.00	23.00	23.00	23.00	23.00	12.50	12.50	8.00	6.00	6.00	23.00	23.00	12.50	12.50	8.00
Si	1.98	2.00	6.53	7.06	7.91	7.99	3.02	3.01	2.98	1.99	2.00	6.96	6.73	3.01	3.01	2.96
Ti	0.42	0.52	0.02	0.01	0.00	0.00	0.02	0.01	0.00	0.00	0.00	0.03	0.03	0.01	0.01	0.00
Al	0.00	0.00	2.60	1.92	2.02	1.94	2.79	2.52	1.00	0.43	0.50	1.86	2.33	2.72	2.11	1.03
Cr	0.12	0.00	0.00	0.00	0.00	0.00	0.00	0.00	0.00	0.00	0.00	0.00	0.01	0.00	0.00	0.00
Fe^{3+}	0.07	0.14	0.33	0.22	0.00	0.00	0.14	0.46	0.01	0.04	0.00	0.23	0.17	0.27	0.89	0.01
Fe^{2+}	0.01	0.00	2.37	1.28	0.90	0.91	0.00	0.01	0.00	0.14	0.12	1.80	1.19	0.00	0.01	0.00
Mn	0.41	0.37	0.00	0.00	0.00	0.00	0.00	0.01	0.00	0.00	0.00	0.00	0.00	0.00	0.00	0.00
Mg	0.52	0.45	1.24	2.59	2.23	2.25	0.02	0.00	0.00	0.42	0.41	2.18	2.59	0.02	0.00	0.00
Ca	0.49	0.52	1.28	1.26	0.11	0.06	2.01	1.98	0.01	0.54	0.49	1.36	1.27	1.95	1.96	0.01
Na	0.00	0.00	1.21	1.05	1.80	1.81	0.00	0.00	1.01	0.45	0.50	1.04	1.27	0.01	0.01	1.01
K	1.98	2.00	0.01	0.04	0.00	0.00	0.00	0.00	0.00	0.00	0.00	0.05	0.08	0.02	0.00	0.00
Sum	4.00	4.00	15.59	15.41	14.98	14.95	8.00	8.00	5.00	4.00	4.00	15.51	15.66	8.00	8.00	5.00

(Continued on following page)

10.3389/feart.2023.1138170

TABLE 2 (*Continued*) Representative compositions of omphacite, amphibole albite and epidote from eclogite at Gaoqiao, western Dabie.

Mineral	Position	GQ-1	GQ-1	GQ-1	GQ-1	GQ-1	GQ-1	GQ-1	GQ-1	GQ-2	GQ-2	GQ-2	GQ-2	GQ-2	GQ-2	GQ-2
		o	o	amp	amp	gl	gl	ep	ep	ab	o	o	amp	amp	ep	ab
		in g	matrix	in g	matrix	matrix	matrix	in g	in g	in g	in g	matrix	in g	matrix	in g	in g
Jd		0.41	0.52								0.42	0.50				
Ae		0.09	0.00								0.03	0.00				
WEF		0.50	0.48								0.55	0.50				

Note: in g, as inclusions in garnet; matrix, as rock-forming minerals in the matrix.

utilized and changed based on the analyzing minerals. The following standards were used: sanidine (K), pyrope garnet (Fe, Al), diopside (Ca, Mg), jadeite (Na), rhodonite (Mn), olivine (Si), rutile (Ti) and apatite (P). Representative results are given in Tables 1, 2.

Elemental mapping was performed using a JEOL JXA-8230 EPMA at the Center for Global Tectonics, School of Earth Sciences, China University of Geosciences (Wuhan). 15 kV accelerating voltage, 100 nA probe current, 1 μm×1 μm pixel size and stage scan model have been utilized during EPMA mapping. The EPMA stage mapping is performed at relatively high probe current to compensate for reduced pixel dwell time, and acquire the higher spatial resolution. All mapping time is spent at the WDS X-ray peak positions. Figure 3 shows the results.

The backscattered electron (BSE) images and energy spectrometer (EDS) analysis were performed at the State Key Laboratory of Geological Processes and Mineral Resources, China University of Geosciences (Wuhan). The equipment used was a FEI Quanta200 scanning electron microscope (SEM) equipped with an EDAX EDS system. The operating conditions have an accelerating voltage of 20 kV, a set spot size of 200–400 nm and an emission current of ~100 μA. The working distance between the BSE probe and the thin section is 11–12 mm.

The whole rock major element analyses were completed in the State Key Laboratory of Geological Processes and Mineral Resources, China University of Geosciences (Wuhan). The samples were analyzed for the major elements using an X-ray fluorescence spectrometer (model ShiMadzuXRF-1800). The X-ray target material is Rh, the power of the test is 2800 W, the analysis voltage is 40 kV, the current is 70 mA, and the raster diameter is 30 mm. Calibration curves used for quantification were produced by bivariate regression of data from ~63 reference materials encompassing a wide range of silicate compositions. The measurement procedure and data quality were monitored by repeated samples (one in eight samples), USGS standard AGV–2 and Chinese National standards GSR–1 and GRS–7. The results are given in Table 3.

4 Petrography and mineral chemistry

Both eclogites GQ–1 and GQ–2 show porphyroblastic texture and have similar mineral assemblages of garnet (25–30 vol%), omphacite (15%–20%), amphibole (20%–25%), epidote (5%–10%), white mica (5%–10%), albite (5%–10%) and quartz (~5%), with accessory rutile, ilmenite, sphene and apatite. Garnet porphyroblast (>5 mm in diameter) is surrounded by oriented fine-grained (<2 mm in diameter) omphacite, amphibole, quartz and albite (Figures 2A, B). At places, residual glaucophane is surrounded by hornblende (Figure 2D) and aggregates of coarse epidote, paragonite and/or albite crosscutting the foliation (Figures 2H, I).

4.1 Garnet

Garnet shows distinct core-rim texture with pink, inclusion-rich core and light, inclusion-rare rim (Figures 2A, E). Inclusions in

TABLE 3 Whole rock compositions (wt%) together with modified bulk rock compositions for eclogite at Gaoqiao, western Dabie.

Samples	Figures	H_2O	SiO_2	Al_2O_3	CaO	MgO	FeO(FeO^T)	K_2O	Na_2O	MnO	O(Fe_2O_3)	P_2O_5
Measured whole rock composition (wt%)												
GQ–1		*	50.059	14.452	9.212	5.562	13.082	0.103	4.434	0.167	*	0.068
GQ–2		*	49.759	14.736	9.670	6.052	12.038	0.155	4.516	0.172	*	0.095
Corrected bulk rock composition for modeling garnet core (mol%)												
GQ–1	Figures 6A,B	excess	54.46	9.27	10.63	9.02	10.71	0.07	4.68	0.15	1.01	
GQ–2	Figures 7A,B	excess	53.96	9.42	11.09	9.78	9.82	0.11	4.75	0.16	0.92	
Calculated effective bulk rock composition for modeling garnet rim (mol%)												
GQ–1	Figures 6C,D	excess	55.30	8.95	10.46	9.50	9.79	0.08	4.99	0.01	0.92	
GQ–2	Figures 7C,D	excess	54.86	9.08	10.95	10.36	8.71	0.12	5.10	0.01	0.82	

garnet core are mainly epidote, muscovite, amphibole, albite, omphacite, quartz and minor small glaucophane and chlorite (Figures 2A, C) and in garnet rim are mainly omphacite, rutile and quartz. Garnet rim is commonly surrounded by corona of sphene, amphibole and albite (Figure 2A) some embayed rims were replaced by quartz, albite and amphibole (Figure 2B).

Element mapping and compositional profiles for large garnet porphyroblasts from both eclogites GQ–1 and GQ–2 show obvious compositional zoning (Figure 3). For eclogite GQ–1, from core to rim, X_{alm} [=Fe2+/(Fe2++Mg+Mn+Ca)] increases from 0.49 to 0.67, and Xpy [=Mg/(Fe2++Mg+Mn+Ca)] from 0.03 to 0.13, while Xgr [=Ca/(Fe2++Mg+Mn+Ca)] decreases from 0.32 to 0.23 and Xspss [=Mn/(Fe2++Mg+Mn+Ca)] from 0.14 to <0.01. For eclogite GQ–2, from core to rim, Xalm increases from 0.49 to 0.65, and X_{py} from 0.03 to 0.13, while X_{gr} decreases from 0.35 to 0.23 and X_{spss} from 0.15 to <0.01. The typical bell-shaped X_{spss} profile was interpreted to represent prograde growth zonation for garnet (Figures 3I, J; Spear, 1993).

4.2 Omphacite

Omphacite mainly occurs as fine rock-forming minerals in the matrix or as inclusions in garnet. At places, omphacites in the matrix were replaced by symplectite of amphibole and albite along rims (Figure 2F). Omphacite in garnet occurs as individual grain (Figure 2C), or together with phengite, paragonite, zoisite and quartz constitute composite mineral aggregates (Figure 2C; Figures 5I–L). In both samples, omphacite has similar compositions. In the matrix, omphacite has slightly higher X_{Jd} [=Na/(Na+Ca)] (0.39–0.53) than the inclusion omphacite (0.32–0.51; Figure 4A).

4.3 Amphibole

Based on microstructure, amphibole can be subdivided into four types: (1) as individual grain or constituting composite aggregates (amp + ep/czo + ab/pa or amp + ab ± o) included in garnet (Figures 2A, E). Both occurrences of amphibole have comparable ^{C}(Al + Fe^{3+} + 2Ti) of 0.71–1.74 p.f.u. and ^{A} (Na + K + 2Ca) of 0.22–0.89 p.f.u. (23 O basis), ranging from ferropargasite to katophorite (Figures 4B,C). At places, residual tiny glaucophane with barroisite rim can be found as inclusions in garnet or being preserved in quartz inclusion in garnet; (2) together with albite as corona rimming garnet (Figure 2A). It is katophorite with ^{C}(Al + Fe^{3+} + 2Ti) of 0.94–1.41 p.f.u. and ^{A} (Na + K + 2Ca) of 0.46–0.78 p.f.u. (Figure 4C); (3) together with albite forming symplectite after omphacite. It has ^{C}(Al + Fe^{3+} + 2Ti) of 0.93–1.27 p.f.u. and ^{A} (Na + K + 2Ca) of 0.48–0.85 p.f.u. and belongs to paragasite (Figure 2F; Figure 4B, C); (4) as porphyroblast in the matrix with glaucophane in the core and winchite in the rim (Figure 2D). The former has ^{C}(Al + Fe^{3+} + 2Ti) of 1.89–1.95 p.f.u., while the later has ^{C}(Al + Fe^{3+} + 2Ti) of 1.20–1.31 p.f.u. and ^{A} (Na + K + 2Ca) of 0.31–0.50 p.f.u. (Figures 4C, D).

4.4 White mica

For both samples, white mica in the matrix occurs as fine-grained phengite (<0.1 mm; Figure 2G) with comparable Si content of 3.27–3.36 p.f.u. (for O=11) (GQ–1) and 3.31–3.39 p.f.u. (GQ–2), or as coarse paragonite (0.2–1 mm) together with epidote and/or albite constituting polyphase mineral aggregates (Figures 2H, I). Phengite in the matrix has Si content slightly decreasing from core to rim and was replaced by paragonite at rim (Figure 2G). Individual phengite inclusions in garnet have lower Si content (3.22–3.34 p.f.u. for GQ–1 and 3.33–3.39 p.f.u. for GQ–2) in garnet core and higher Si content (3.45–3.53 p.f.u. for GQ–2) in garnet rim (Figure 4E). Phengite constituting polymineralic aggregates in garnet commonly has relatively low Si contents (3.34–3.42 p.f.u. for GQ–1 and 3.34–3.47 p.f.u. for GQ–2). Paragonite inclusion in garnet rarely occurs as individual grain but together with ep/czo ± amp ± ab ± q ± ph constituting polymineralic aggregates, showing rhombic or rectangular shape (Figures 2C, E; Figure 4E; Figures 5A–K).

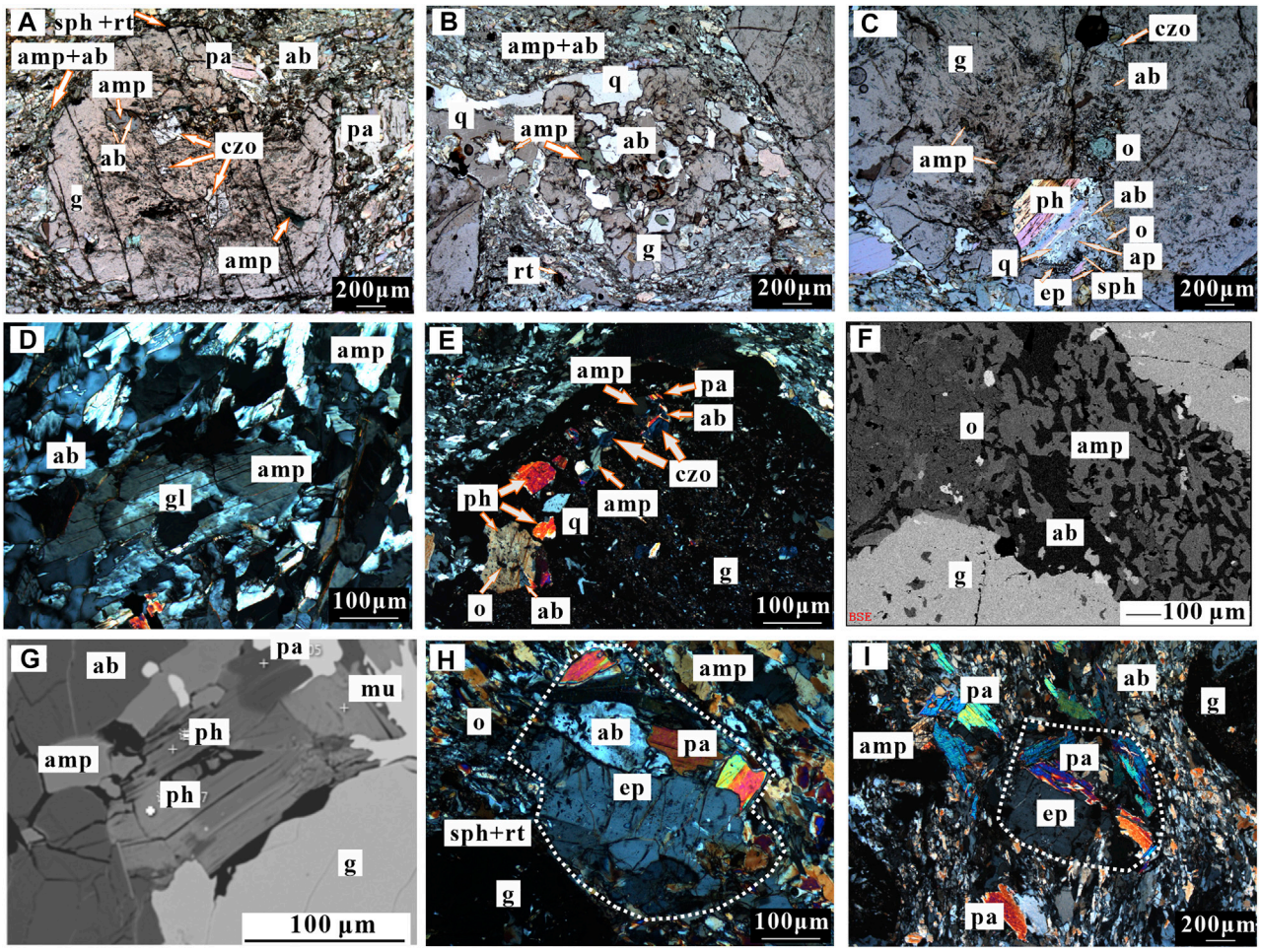

FIGURE 2
Photomicrographs showing texture features of eclogite at Gaoqiao, western Dabie under plan-polarized light **(A–C)**, cross polarized light **(D–I)** and in BSE images **(F,G)**. **(A)** Porphyroblastic garnet showing pink, inclusion-rich core and light-colored, rare inclusion rim. In garnet core, inclusions are mainly clinozoisite, paragonite, amphibole, quartz and ilmenite/sphene. Whereas in garnet rim, inclusions are mainly omphacite, quartz and amphibole. At places, amphibole + albite and sphene replaces garnet along rim. **(B)** Relic garnet eroded by quartz, albite and amphibole. **(C)** Polyphase mineral inclusions of phengite, epidote, quartz, albite, amphibole, and omphacite in garnet, interpreted to be pseudomorphs after lawsonite. **(D)** Amphibole porphyroblast in the matrix with glaucophane relics in the core. **(E)** Inclusions of phengite, paragonite, albite, clinozoisite and quartz in garnet rim. **(F)** Omphacite in the matrix replaced by symplectite of amphibole + albite. **(G)** High-Si phengite (darker, at core) in the matrix replaced by low-Si phengite (lighter, at rim) and paragonite **(H,I)**. In the matrix, aggregates of coarse-grained epidote, paragonite and albite showing box shape, interpreted to be pseudomorphs after lawsonite.

4.5 Other minerals

In both samples, epidote in the matrix has comparable pistacite (Ps) ($Fe^{3+}/(Fe^{3+}$ + Al)) of 0.16–0.3 (Figures 2H,I; Table 2). Epidote included in garnet is mainly clinozoisite with Ps of 0.02–0.09 (Figure 2A; Figures 4A–H; Table 2). Plagioclase in both samples is albite with $Ab_{0.99\text{-}1}$.

4.6 Pseudomorphs after lawsonite

In both eclogites GQ–1 and GQ–2, detailed petrographic observations and BSE images have shown that ubiquitous composite mineral aggregates (50–500 μm in diameter) showing distinct rectangular and/or rhombic shapes were developed. They occur either as inclusions in garnet (Figure 5) or in the matrix crosscutting the foliation (Figures 2H,I). Based on variations on mineral assemblages, we can subdivide those polymineralic aggregates into four types: (1) comprising ep/czo + pa/ab (Figures 2H,I; Figures 5A–D), (2) dominated by amp-bearing mineral aggregates of czo + pa/ab + amp (Figures 5E–H), (3) dominated by ph-bearing mineral aggregates of ep/czo + pa/ab + ph (Figures 5I–K) and (4) dominated by quartz with relics of omphacite, epidote and sphene (Figure 5L). These polymineralic aggregates are interpreted to be pseudomorphs after lawsonite based on their orthorhombic polyhedral shapes (Castelli et al., 1998; Mattinson et al., 2006; Zhang J. X. et al., 2007; Wei et al., 2010; Angiboust et al., 2012; Guo et al., 2013; Liu et al., 2013; Du et al., 2014; Orozbaev et al., 2015; Hamelin et al., 2018; Ren et al., 2018).

The above petrographic observations and mineral chemistry show that four metamorphic stages can be inferred for eclogite at Gaoqiao, western Dabie. The prograde stage is evidenced by garnet core and its inclusions of o + gl + ph + q + ru + law (pseudomorphs) ± ep. The peak stage is evidenced by garnet rim, its inclusions of o + ph + gl + q + law (pseudomorphs) + ru and rock-forming minerals of o + ph + gl +q + law (pseudomorphs) in the matrix. The early retrograde stage is evidenced by the breakdown of lawsonite to form polymineralic aggregates, glaucophane to form amphibole, garnet to form amphibole, and/or epidote and omphacite to form symplectite. Therefore, the mineral assemblages are inferred to be cpx + amp + pl + ph + q + ru + ep ± pa. The late retrograde stage is evidenced by coarse amphibole, epidote and albite in the matrix and albite replacing paragonite and/or phengite in polymineralic aggregates in garnet. Mineral assemblage for this stage was inferred to be amp + ep + ab + q + ilm/sph.

5 Phase equilibrium modelling

5.1 Methods

To constrain *P–T* evolution and explore factors influencing the formation and breakdown of lawsonite for eclogite at Gaoqiao, western Dabie, phase equilibrium modeling was performed. We use Thermocalc 3.33 software (Powell et al., 1998) and the associated ds55 database (Holland and Powell, 1998; updated November 2003) in the chemical system NCKMnFMASHO (Na_2O–CaO–K_2O–MnO–FeO–MgO–Al_2O_3–SiO_2–H_2O–O) for modeling. *A–x* relationships used are as follows: garnet (White et al., 2005), clinopyroxene (Green et al., 2007), amphibole (Diener and Powell, 2012), epidote and talc (Holland and Powell, 1998), chlorite (Holland et al., 1998), muscovite (Coggon and Holland, 2002) and plagioclase (Holland and Powell, 2003). Lawsonite, kyanite, quartz/coesite, and H_2O are considered as

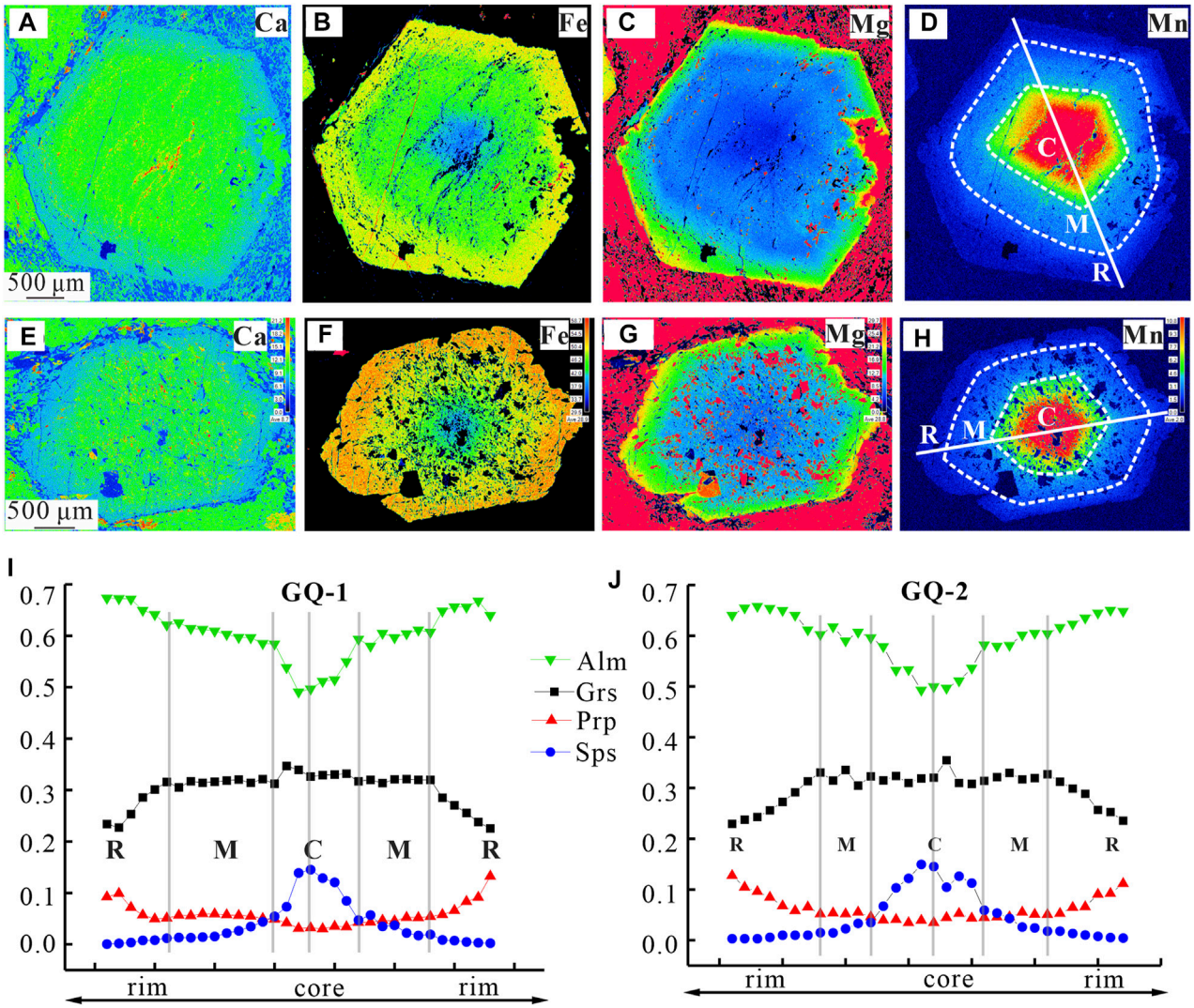

FIGURE 3
(A–H) X-ray element mapping for garnet from the eclogite GQ–1 **(A–D)** and GQ–2 **(E–H)** at Gaoqiao, western Dabie, respectively. **(I,J)** Travers of point analyses for garnet from the eclogite GQ–1 and GQ–2, respectively. **(C)** represents garnet core, M represents garnet mantle, R represents garnet rim.

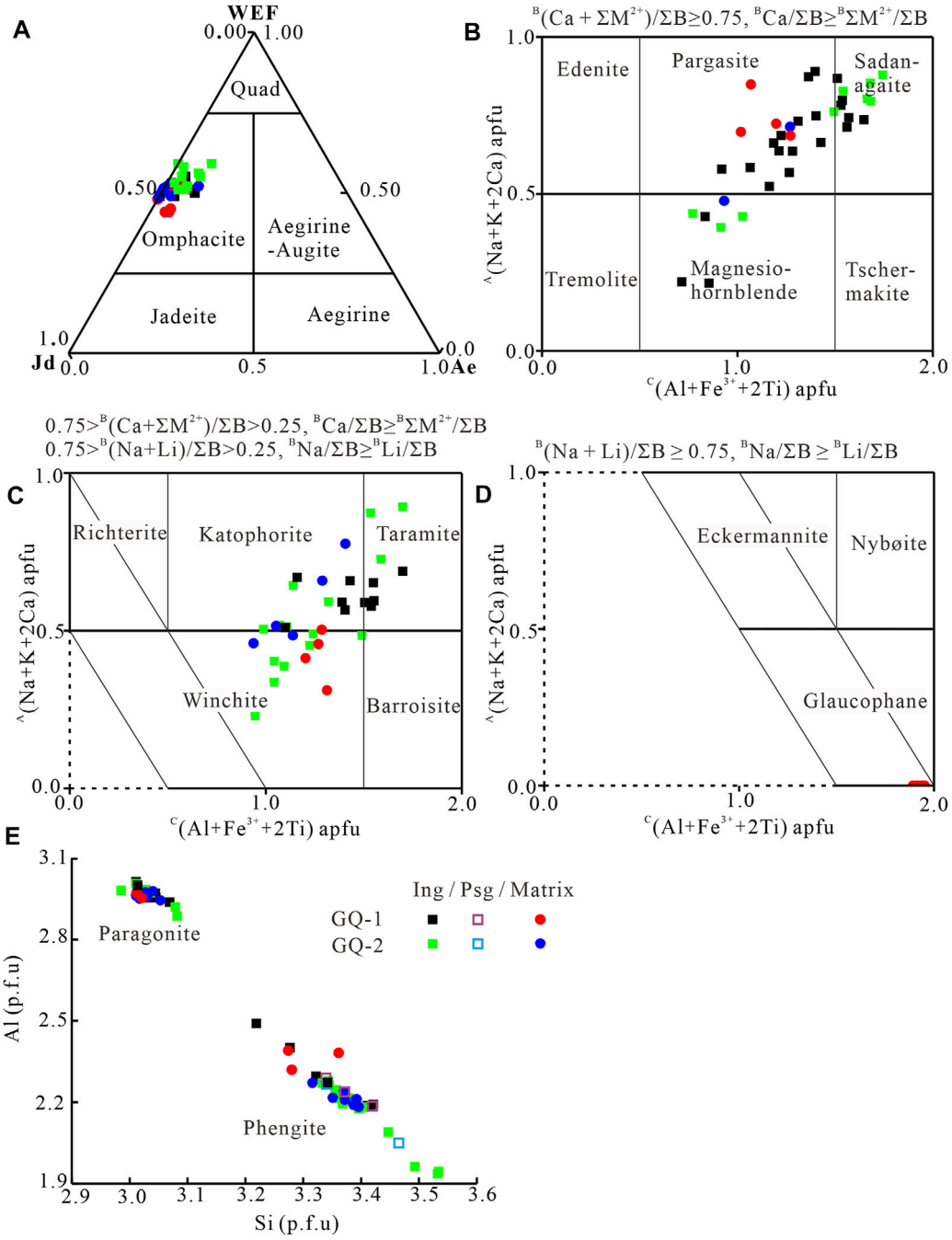

FIGURE 4
Compositions of omphacite **(A)**; after Morimoto, 1988), amphibole **(B–D)**; after Hawthorne et al., 2012) and phengite and paragonite **(E)** from the eclogite GQ–1 and GQ–2 at Gaoqiao.

pure phases. H_2O was set to be excess considering numerous hydrous minerals (e.g., epidote, lawsonite, white mica, amphibole and inferred lawsonite) included in garnet. Oxygen (equal to Fe_2O_3 in mol%) values in the bulk compositions were calculated based on the Fe^{3+}/FeO_T values in the whole rock compositions from previous studies in the same outcrop (Liu et al., 2004a; Cheng et al., 2010).

Whole rock compositions obtained by XRF were used for modeling after CaO, FeO_T and MgO correction for CO_2 content in calcite and P_2O_5 content in apatite (Table 3). Considering garnet has distinct growth zoning (Figure 3), the growth of garnet may lead to fractionation of the bulk rock composition (Evans, 2004). In this study, we used the corrected XRF bulk rock composition to model *P–T* conditions for garnet core growth. For modeling garnet rim growth, we get the effective bulk rock composition using the principle of Rayleigh fractionation to deduct garnet core composition from the corrected XRF bulk rock composition following the method recommended by Evans (2004). The results are shown in Table 3. In addition, considering that different oxides in the bulk composition

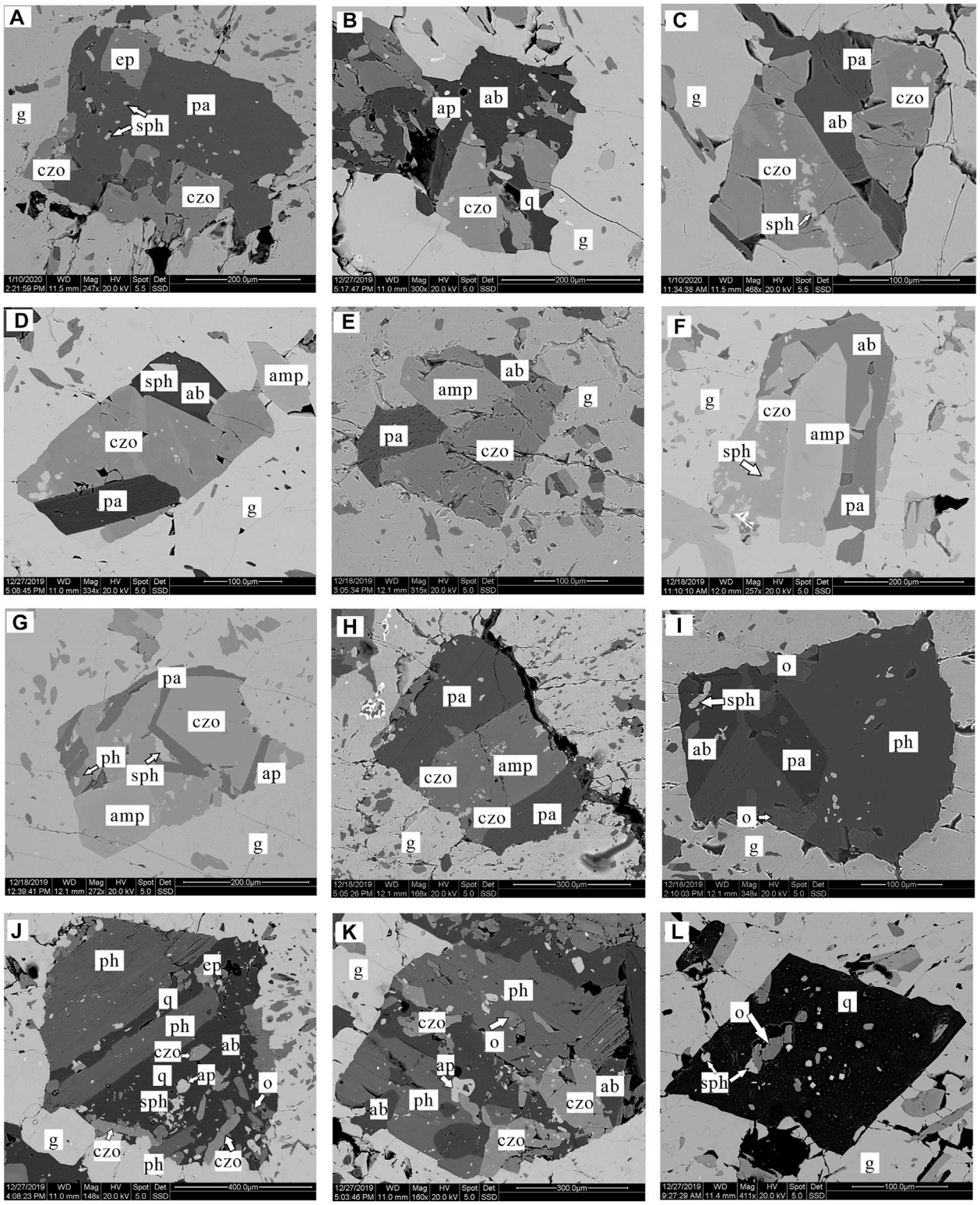

FIGURE 5
Backscattered electron images showing various composite inclusions in garnet define rectangular or rhombic shapes, maybe pseudomorphs after lawsonite. **(A–D)** composite inclusions dominated by ep/czo + pa/ab; **(E–H)** amp-bearing composite inclusions dominated by czo + pa/ab + amp; **(I–K)** ph-bearing composite inclusions dominated by ep/czo + pa/ab + ph; **(L)** quartz with relics of omphacite, epidote and sphene showing rhombic shape.

may affect the formation and stability of lawsonite, we systematically calculated *P/T*–H_2O, O (Fe^{3+}), X_{MgO} [MgO/(MgO+FeO)], XCaO [CaO/(CaO+MgO+FeO+MnO+Na2O)], XNa2O [Na2O/(CaO+Na2O)] and XAl2O3 [Al_2O_3/(Al_2O_3+CaO+Na_2O)] pseudosections at specific *P* and *T* conditions, respectively, using the bulk rock compositions in Supplementary Table S1.

5.2 *P–T* pseudosections using the corrected XRF bulk rock composition

For eclogites GQ–1 and GQ–2, phase diagrams constraining *P–T* conditions for garnet core and mantle growth were calculated under the NCKMnFMASHO system using the bulk rock compositions in Table 4 for given *P–T* ranges of 400°C–600°C and 10–30 kbar (Figures 6A, B; Figures 7A,B). The results show that, the *P–T* pseudosections are dominated by di- and trivariant fields, with few quadri- and quinivariant fields. Lawsonite-bearing phase assemblages are present at high *P* fields of 11–30 kbar at 400°C–600°C and epidote-bearing phase assemblages are present at low *P* fields of <20 kbar and 400°C–600°C. Because of slightly different bulk rock composition, the phase diagram for GQ–1 (Figure 6A) has larger di-bearing but smaller q-absent fields than that for GQ–2 (Figure 7A).

Compositional isopleths for X_{gr} and X_{py} in garnet and Si content in phengite have been calculated for the concerned *P–T* range (Figure 6B; Figure 7B). In the lawsonite-bearing phase assemblage fields, isopleths for X_{gr} in garnet have a flat slope and decrease with pressure, while isopleths for X_{py} have a negative steep to vertical slope and increase with temperature (Figure 6B; Figure 7B. On the other hand, in the epidote-bearing phase assemblage fields, both X_{gr} and X_{py} isopleths have negative moderate slopes, X_{gr} decreases while X_{py} increases with temperature (Figure 6B; Figure 7B). Isopleths for Si content in phengite have negative moderate slope and increases with pressure. Besides, the calculated H_2O mode isopleths have a steep slope and roughly decrease with temperature (Figure 6B; Figure 7B).

For both eclogites GQ–1 and GQ–2, the observed inclusions of omphacite, glaucophane, amphibole, lawsonite pseudomorphs of ep + pa, phengite, chlorite and quartz in garnet core to mantle correspond to the modeled phase assemblages of g + o + gl + law ± chl ± ep + q + mu + H_2O (Figure 6A; Figure 7A). In these phase assemblage fields, the measured X_{spss} in garnet inner core (0.150–0.035 for both GQ–1 and GQ–2) and X_{gr} (from 0.347 to 0.313 for GQ–1 and from 0.324 to 0.308 for GQ–2) and X_{py} (from 0.049 to 0.030 for GQ–1 and from 0.053 to 0.034 for GQ–2) from garnet core to mantle have constrained a segment of the prograde *P–T* evolution from 19 to 20 kbar, 470°C–475°C to 20–21 kbar, 510°C (Figure 6B; Figure 7B). However, in the phase assemblage fields of g + o + gl + ep + chl ± law + q + mu + H_2O the measured Si content (3.22–3.34 p.f.u for GQ–1 and 3.33–3.39 p.f.u for GQ–2) in phengite from garnet core corresponds to pressure of 10–18 kbar at 400°C–510°C. The slightly low pressure may either be disequilibrium between garnet core and the included phengite, or phengite composition being reset during retrogression considering paragonite/albite replacing phengite inclusions at some places.

In GQ–1, the highest Si of 3.42 p.f.u. was measured for phengite in the garnet rim. At a peak temperature of 555°C, the Si isopleths of phengite is limited to 22.5 kbar in the peak mineral combination g+o+gl+law+q+mu+H_2O, which is about 2 kbar lower than the pressure limited by X_{gr} (Figures 6B, D). In GQ–2, the highest Si of 3.53 p.f.u. was measured for phengite in the garnet rim. At a peak temperature of 555°C, the Si isopleths of phengite is limited to 23.5 kbar in the peak mineral combination g+o+gl+law+q+mu+H_2O, which is about 1.5 kbar lower than the pressure limited by X_{gr} (Figures 7B, D). Based on the isopleths of saturated water content of the relevant mineral assemblage (Figure 6B; Figure 7B), the *P–T* path of the metamorphism process crosses the isopleths of the decrease of saturated water content and evolves in the direction of decreasing water content. It shows that H_2O exists in the process of metamorphism and the evolution of minerals is dominated by dehydration (Guiraud et al., 2001).

5.3 *P–T* pseudosections using an effective bulk rock composition

For eclogites GQ–1 and GQ–2, phase diagrams constraining *P–T* conditions for garnet rim0. growth were calculated under the NCKMnFMASHO system using the effective bulk rock compositions in Table 3 for the given *P–T* ranges of 400°C–600°C and 10–30 kbar (Figures 6C, D; Figures 7C, D). The results show that the topology and phase relations in Figure6C; Figure 7C are similar to those of Figure 6A; Figure 7A, except that garnet is absent in the fields *p* <18 kbar and *T* <485°C. Besides, in Figure 7D, actinolite is present in the modeled phase assemblage fields of 12–28 kbar and 400°C–485°C.

In the phase assemblage field of g + o + gl + law + mu + q + H_2O, *P–T* conditions constrained by isopleths of the measured X_{py} (0.051–0.132 for GQ–1 and 0.052–0.127 for GQ–2) and X_{gr} (0.316–0.234 for GQ–1 and 0.331–0.230 for GQ–2) in garnet rim are ~25 kbar and 530C–555°C. Those values are interpreted to represent P_{max}–*T* conditions for eclogite at Gaoqiao, western Dabie. The maximum Si content of 3.53 p.f.u. In phengite included in garnet rim from eclogite GQ–2 corresponds to *P* of 22–24 kbar at 530°C–555°C, slightly lower than that constrained by garnet rim compositions. Lower Si content of 3.27–3.39 p.f.u. for phengite in the matrix (Figure 4E) may indicate compositional reset of phengite during exhumation after the *Pmax* stage (Xia et al., 2020).

The observed mineral assemblage of g + o + amp + ep + q + ph + pa in the matrix corresponds to the modeled phase assemblage of g + o + hb + ep + q + ph + pa + H_2O with *P–T* regime of 10–16 kbar, 520°C–555°C (Figure 6D; Figure 7D). Combined with lawsonite breakdown to form composite inclusions of ep/czo + pa/ab + ph, low Si contents of 3.27–3.39 p.f.u. In phengites in the matrix or constituting lawsonite pseudomorphs in garnet, we infer the early retrograde stage may follow an isothermal decompression process during subsequent exhumation from the P_{max} stage. In the phase assemblage field of g + o + gl + law + q + mu + H_2O, the retrograde *P–T* path may firstly be tangential to the calculated isopleths for H_2O mode content in relevant hydrous phases. Then, the *P–T* path crossed lawsonite-epidote transition fields at 19 kbar at 550C–560°C. The breakdown of lawsonite *via* the reaction law + o→ ep + gl ± pa + H_2O would release a significant amount of H_2O and the *P–T* path crossed the H_2O decrease contours with H_2O content in the

10.3389/feart.2023.1138170

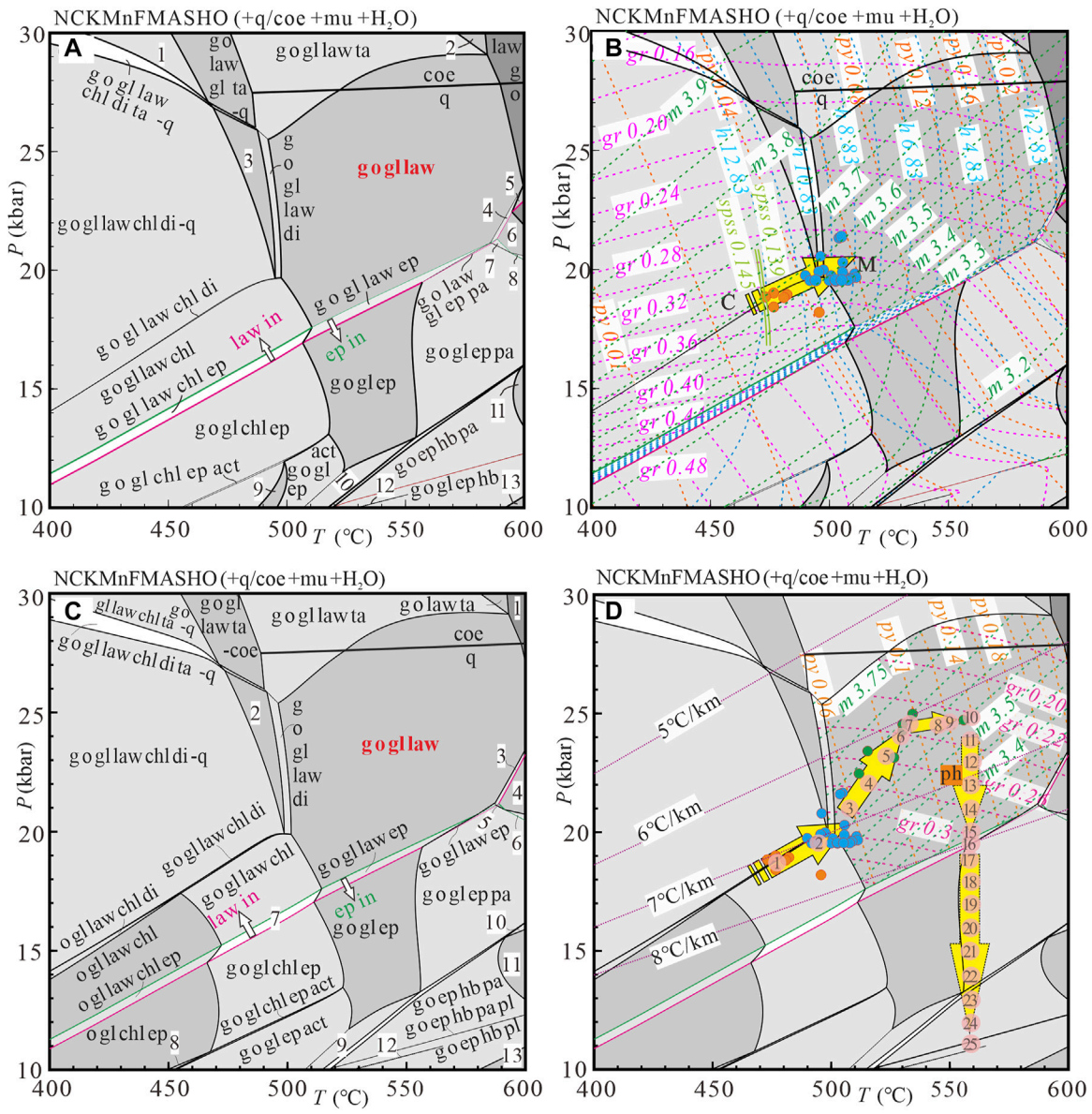

FIGURE 6
P–T pseudosections for the eclogite GQ–1 using primary bulk rock composition **(A,B)** and effective bulk rock composition **(C,D)** in Table 4 gr represents calculated isopleth for grossular in garnet, py represents calculated isopleth for pyrope in garnet, m represents calculated isopleths for Si in phengite and h represents calculated isopleths for H_2O modal content saturated for relevant phase assemblages. Yellow arrows represent inferred *P–T* evolution from the prograde to peak, then to retrograde stages. C, M, R1 and R2 represent compositions of garnet core, mantle and rim (inner rim and outer rim), respectively. In figure **(D)**, the calculated geothermal gradient during the prograde process is 6°C–7°C/km (assuming 2.8 km/1 kbar, after Wei et al., 2010). In **(A)**, the number represents: 1. g o gl law chl ta -q, 2. g o law ta, 3. g o gl law di -q, 4. g o gl law ky, 5. g o glaw ky, 6. g o gl ky, 7. g o gl ep ky, 8.g o gl pa ky, 9. g o gl ep act -q, 10. g o gl ep hb, 11. g o hb pa, 12. g o di ep hb pl, 13. g hb pL di. In **(C)**, the number represents: 1. g o law, 2. g o gl law di -q, 3. g o gl law ky, 4. g o gl ky, 5. g o gl ep ky, 6. g o gl pa ky, 7. g o gl law chl ep, 8. o gl chl ep act, 9. g o gl ep hb, 10. g o gl hb pa, 11. g o hb pa, 12. g o di ep hb pl, 13. g di hb pl.

bulk rapidly decreasing from 1.00 wt% to 0.52 wt%. When the *P–T* path entered the fields of g + o + gl/hb + ep ± pa + q + H_2O with p <13 kbar, amphibole developed at the expense of glaucophane, and caused overprint of epidote-amphibolite facies metamorphism. Note that following this *P–T* path, H_2O contours increased, implying additional external fluid may enter the rock system. Further decompression to 11 kbar led to the formation of albitic plagioclase after paragonite.

5.4 *P/T–X* pseudosections modeling the influence of various oxides in bulk composition on the stability of lawsonite

To evaluate influence of the contents of H_2O, O (Fe^{3+}) and other oxides (MgO, CaO, Na_2O and Al_2O_3) in the bulk rock composition on the stability of lawsonite during metamorphic evolution, we calculated a series of *P/T-X* phase diagrams for eclogite GQ–1 (Supplementary

10.3389/feart.2023.1138170

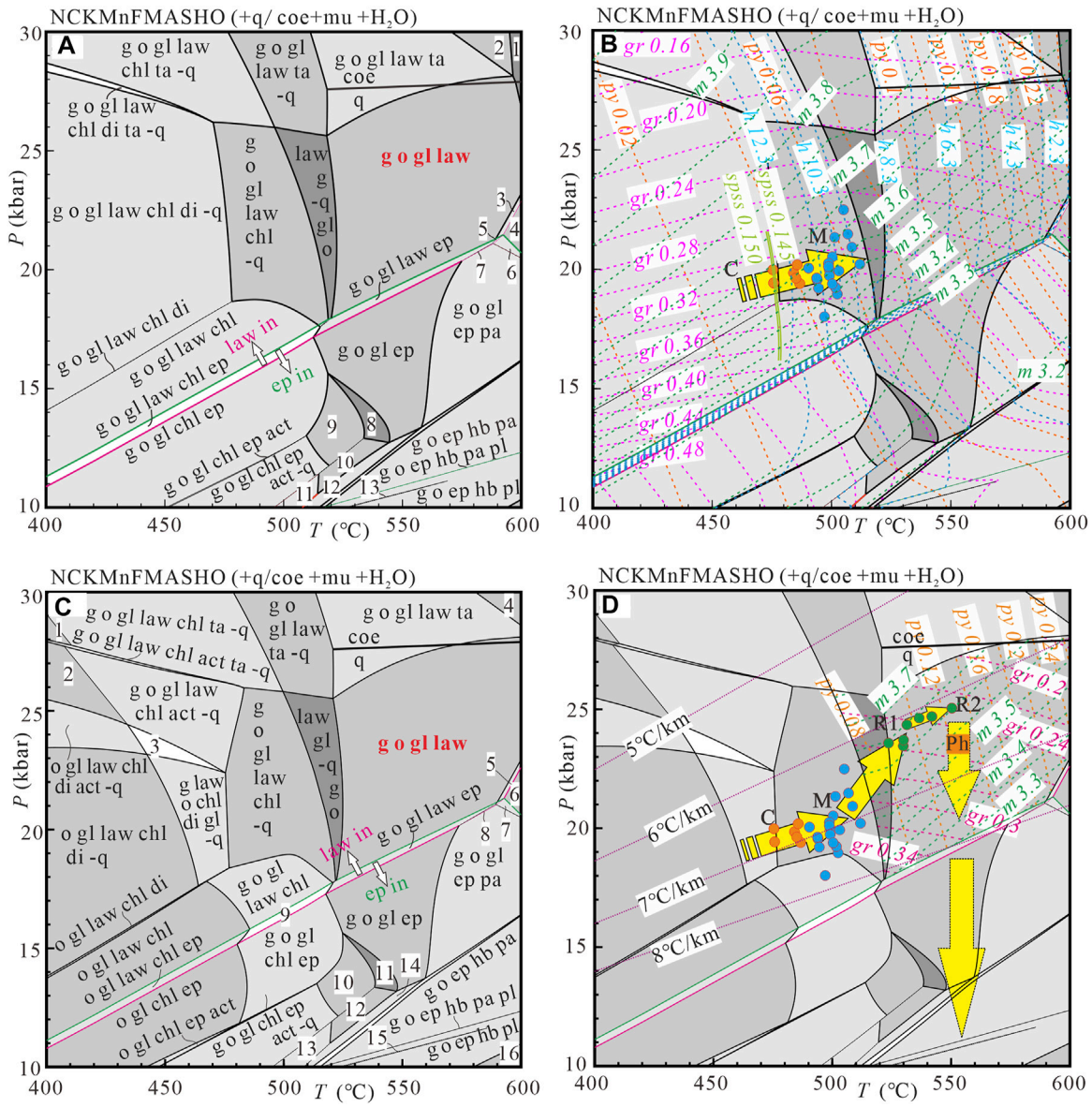

FIGURE 7
P–T pseudosections for the eclogite GQ–2 using primary bulk rock composition **(A,B)** and effective bulk rock composition **(C,D)** in Table 4. In **(A)**, the number represents: 1. g o law, 2. g o law ta, 3. g o gl law ky, 4. g o gl ky, 5. g o gl law ep ky, 6. g o gl ep ky, 7. g o gl law ep pa, 8.g o gl ep -q, 9. g o gl chl ep -q, 10. g o gl ep hb -q, 11. g o gl ep act hb -q, 12. g o gl ep hb, 13. g o ep hb pl di. In **(C)**, the number represents: 1. o gl law chl ta -q, 2. o gl law chl act -q, 3. g o gl law chl di act -q, 4. g o law ta, 5. g o gl law ky, 6. g o gl ky, 7. g o gl ep ky, 8. g o gl law ep pa, 9. g o gl law chl ep, 10. g o gl chl ep -q, 11. g o gl ep -q, 12. g o gl ep hb -q, 13. g o gl ep act hb -q, 14. g o gl ep hb, 15. g o ep hb di pl, 16. g hb pL di. Others are the same to Figure 6.

Figures S1–S6). *T–X* (at p = 25 kbar) and *P–X* (at T = 550°C) pseudosections were calculated under the NCKMnFMASHO system using the compositions in Supplementary Table S1 for the given T ranges of 400°C–600°C or P ranges of 10–30 kbar, respectively.

5.4.1 *P/T*–H_2O pseudosections

Supplementary Figure S1 shows that, in both T–M_{H2O} and P–M_{H2O} pseudosections, in H_2O-present fields, phase relations do not change with the increase of H_2O and lawsonite is present at T <621°C at p = 25 kbar (Supplementary Figure S1A) or at p >19 kbar at T = 550°C (Supplementary Figure S1B). In Supplementary Figure S1A in H_2O-absent fields, lawsonite is absent at M_{H2O} < 0.144 wt% while in Supplementary Figure S1B, when p >19 kbar, lawsonite is absent at M_{H2O} < 0.573 wt%.

5.4.2 *P/T*–O pseudosections

Supplementary Figure S2A shows that lawsonite is present at T <625°C at p = 25 kbar. At O <0.72, lawsonite-bearing phase

assemblage fields reduce when O decreases. In Supplementary Figure S2B, in the range of O = 0–3, lawsonite is present at p >19 kbar at T = 550°C and changes little when O varies.

5.4.3 $P/T–X_{MgO}$ pseudosections

The calculated $T–X_{MgO}$ phase diagram at p = 25 kbar (Supplementary Figure S3A) shows that at X_{MgO} <0.39, the stability field for lawsonite-bearing phase assemblages reduces when X_{MgO} decreases. At X_{MgO} >0.39, lawsonite stability field changes little when X_{MgO} increases. Similarly, in $P–X_{MgO}$ phase diagram at 550°C (Supplementary Figure S3B), lawsonite stability field reduces when X_{MgO} decreases at X_{MgO} <0.26, but changes little when X_{MgO} increases at X_{MgO} >0.26.

5.4.4 $P/T–X_{CaO}$ pseudosections

The calculated $T–X_{CaO}$ phase diagram at p = 25 kbar (Supplementary Figure S4A) shows that lawsonite stability field increases when X_{CaO} increases and at X_{CaO} >0.36, lawsonite is stable in the T range of 400°C–650°C. In Supplementary Figure S4B, the calculated $P–X_{CaO}$ phase diagram at T = 550°C shows that lawsonite-bearing phase assemblages are stable at p >19 kbar and the variation of X_{CaO} has little influence on the stability of lawsonite.

5.4.5 $P/T–X_{Na2O}$ pseudosections

Supplementary Figure S5A shows that in the $T–X_{Na2O}$ phase diagram calculated at 25 kbar, lawsonite stability field decreases distinctly when X_{Na2O} increases from 0.1 to 0.5. On the other hand, in the $T–X_{Na2O}$ phase diagram calculated at 550°C, lawsonite stability field shows little change at p <20 kbar when X_{Na2O} changes from 0.1 to 0.44. However, at X_{Na2O} >0.44, lawsonite is absent in the pressure range of 10–30 kbar.

5.4.6 $P/T–X_{Al2O3}$ pseudosections

In Supplementary Figure S6A for $T–X_{Al2O3}$ phase diagram calculated at p = 25 kbar, lawsonite is stable at T <620°C and its stability field increases when X_{Al2O3} increases from 0.3 to 0.61. At X_{Al2O3} >0.61, lawsonite stability field changes little to X_{Al2O3}. In Supplementary Figure S6B for $P–X_{Al2O3}$ phase diagram calculated at T = 550°C, lawsonite is absent at X_{Al2O3} <0.50. At X_{Al2O3} >0.50, lawsonite is stable at p >19.5 kbar and its stability field changes little when X_{Al2O3} increases.

6 Discussion

61 Retracing lawsonite composition

Based on the acquaintance that pseudomorphs after lawsonite commonly contain Na^+- or K^+-phases (e.g., paragonite, albite, phengite, etc.), lawsonite breakdown reactions should take place in a dominantly open system (Barnicoat and Fry, 1986; Pognante, 1989; Zhang J. X. et al., 2007; Angiboust and Agard, 2010; Angiboust et al., 2012; Orozbaev et al., 2015). Therefore, reconstructing the original lawsonite composition from polyphase pseudomorphs requires consideration of Na^+ or K^+ migration within fluid (Angiboust and Agard, 2010; Hamelin et al., 2018; Xia et al., 2020). In this study, we calculate the original lawsonite composition using mass balance by combing modal ratios of individual mineral in the polyphase aggregates and their compositions, as recommended by previous studies (e.g., Angiboust and Agard, 2010; Orozbaev et al., 2015; Hamelin et al., 2018). Firstly, we used mass balance (least square method; software PCalc 2.3 by Godard (2010)) for three represented composite inclusions of czo/ep + pa/ab ± amp in Figures 5C–E to establish lawsonite breakdown reactions. The balanced reactions are as follows.

1.000law +0.038o + 0.148Na^+ + 0.084Si^{4+} = 0.511ep + 0.203pa + 2H_2O (reaction 1; Figure 5C)

1.000law +0.242o + 0.754Na^+ + 0.016Fe/Mg = 0.557ep + 0.168pa +0.036gl + 2H_2O (reaction 2; Figure 5D)

1.000law +0.216o + 0.069Na^+ + 0.013Fe/Mg = 0.552ep + 0.166pa +0.031gl + 2H_2O (reaction 3; Figure 5E)

The mass balance calculations show that the molar ratios of ep and pa are between 2.52 and 3.32. Then, two-dimensional quantitative estimation of the volume ratios of ep/czo and pa/ab (Figures 5C–E) was performed using Image-ProPlus 6.0 image processing software. Since albite is interpreted to be transformed from paragonite, the area of albite in the composite inclusions is classified as paragonite during counting. Ignoring all voids and rare accessory minerals, the volume ratios of ep/czo and pa/ab are between 2.19 and 2.51, similar to the molar ratios of epidote and paragonite in reactions (1), (2) and (3) based on their similar molar volumes (Holland & Powell, 2011).

Thirdly, combined with the volume ratios, densities and compositions of the minerals in the composite inclusions, the bulk composition of the pseudomorphs was estimated using the method of Orozbaev et al. (2015). The restricted lawsonite compositions are shown in Table 4. The results show that, SiO_2, Al_2O_3 and CaO contents in the reconstructed lawsonite composition are very similar to that of ideal lawsonite while FeO and Na_2O contents are slightly higher (Table 4). Reasons could be uncertain in estimating volume ratio of minerals in the composite inclusions, or the introduce of Na^+, Fe and Mg due to H_2O migration during lawsonite breakdown. Tiny fractures developed around the composite inclusions (Figure 5) may have been acted as pathways for fluid ingress or egress (Lü et al., 2019). Nonetheless, the proportions of SiO_2, Al_2O_3 and CaO are very similar to that of ideal lawsonite (Table 4).

6.1.1 $P–T$ evolution

Based on the above petrographic observations, mineral chemistry and phase equilibrium modelling, a complete $P–T$ path comprising the later prograde, P_{max}, initial decompression and late retrograde stages have been inferred for eclogite at Gaoqiao, western Dabie.

6.1.2 Prograde to peak stages

A segment of the late prograde stage metamorphic evolution was inferred based on inclusions in garnet core and garnet core composition showing distinct growth zoning. Phase equilibrium modeling (Figures 6, 7) shows that, in the modeled phase assemblage fields g + o + gl + law ± chl ± ep ± q± di + mu + H_2O, garnet inner core composition (X_{gr} =0.347–0.308, X_{py} = 0.053–0.030 and X_{spss} =0.150–0.035) corresponds to a $P–T$ regime of 19–20 kbar,

10.3389/feart.2023.1138170

TABLE 4 Recalculated lawsonite composition (wt%) from the composite inclusions in garnet (Figures 5C–E) from eclogite at Gaoqiao.

Samples	Figure 5C	Figure 5C	Figure 5D	Figure 5D	Figure 5D	Figure 5E	Figure 5E	Figure 5E	Figure 5C	Figure 5D	Figure 5E	Figure 5C	Figure 5D	Figure 5E	Reference	Reference
Minerals	ep	pa	ep	pa	amp	ep	pa	amp	PMA–1	PMA–2	PMA–3	PMA–1	PMA–2	PMA–3	law	law
SiO_2	38.83	47.67	39.09	48.40	42.59	39.33	48.37	48.18	41.32	42.06	43.11	37.87	38.56	39.54	38.33	39.81
TiO_2	0.20	0.03	0.25	0.05	0.18	0.19	0.02	0.13	0.15	0.19	0.14	0.14	0.17	0.13	0.06	0.06
Al_2O_3	30.19	39.45	30.60	39.30	14.93	30.94	38.91	11.02	32.80	31.78	28.22	30.06	29.14	25.88	31.13	31.57
Cr_2O_3	0.01	0.03	0.00	0.00	0.00	0.00	0.00	0.00	0.02	0.00	0.00	0.01	0.00	0.00	0.04	0.01
FeO	2.56	0.38	2.16	0.29	21.38	2.22	0.80	15.01	1.95	3.24	4.72	1.78	2.97	4.33	0.84	1.18
MnO	0.00	0.00	0.01	0.00	0.02	0.07	0.03	0.02	0.00	0.01	0.05	0.00	0.01	0.05	0.03	0.03
MgO	0.16	0.29	0.14	0.24	5.63	0.12	0.15	10.71	0.20	0.63	2.44	0.18	0.58	2.24	0.03	0.23
CaO	23.84	0.22	24.23	0.25	8.61	24.30	0.18	7.82	17.19	16.03	15.78	15.75	14.70	14.47	17.5	17.08
Na_2O	0.00	6.64	0.00	6.15	3.85	0.03	5.60	3.95	1.87	2.09	2.02	1.71	1.92	1.86	0.02	0.00
K_2O	0.01	0.89	0.00	0.40	0.25	0.00	0.73	0.18	0.26	0.14	0.19	0.24	0.12	0.17	0.00	0.01
Total	95.83	95.60	96.48	95.10	97.43	97.19	94.79	97.03	95.74	96.16	96.67	87.74	88.16	88.67	87.97	89.99

Deduct 8 wt% H_2O

470C–475°C (Figures 6B; Figures 7B), interpreted to represent the initial growth of garnet. The decease of X_{gr} and increase of X_{py} from garnet outer core to rim further correspond to a *P–T* evolution to ~20 kbar, 500C–505°C and then to ~25 kbar, 530C–555°C. Notably, for both eclogites GQ–1 and GQ–2, maximum pressures constrained by the maximum Si content in phengite (22.5 kbar at 510°C–560°C for GQ–1; 23.5 kbar at 520°C–550°C for GQ–2) are slightly lower than those constrained by the garnet outer rim compositions (Figures 6B, C; Figures 7B, C). Possible reasons could be: (1) systematic uncertainties propagated from each endmember enthalpy in the dataset (±0.4 kbar within two sigma error); (2) random uncertainties propagated from the analytical uncertainties for EPMA of phengite and garnet (within ~2% relative); (3) not found phengite with higher Si content during petrographic observations; or (4) possible re-equilibration of Si in phengite during retrogression (Liu et al., 2004a; Jahn et al., 2005; Liu et al., 2006; Wei et al., 2010).

The prograde to peak metamorphism shows a two-stage *P–T* evolution defined by the slope of the thermal gradient of the *P–T* path. The first stage *P–T* path with a gentle positive slope is dominated by heating and slight increase in pressure, following a geothermal gradient of ~7°C/km (Figure 6D; Figure 7D). On the other hand, the second *P–T* path shows a moderate positive slope with geothermal gradient decreasing to ~6°C/km. Such a *P–T* path pattern has been reported by Wei et al. (2010) for eclogite in the Xinxian UHP unit in western Dabie and was interpreted to reflect a change of subduction rate from slow to fast.

6.1.3 Retrograde stages

During initial exhumation, lawsonite broke down to form composite mineral aggregates of ep/czo + pa/ab + other minerals in the matrix or as inclusions in garnet. Phase equilibrium modeling shows that the transition of lawsonite to ep ± pa occurred at 19 kbar and 550°C–560°C. This pressure is consistent to *P* constrained by isopleths of Si in phengites from the composite inclusions (3.33–3.41 p.f.u.) or from the aggregates in the matrix (3.28–3.39 p.f.u.), the former gives *P* of ~20 kbar at 555°C and the later of ~19 kbar at 555°C. Therefore, we estimate the early decompression stage subsequentially passed through the lawsonite-present field of g + o + gl + law + mu + q + H_2O, lawsonite–epidote coexistent fields of g + o + gl + law + ep + mu + q + H_2O ± pa and lawsonite-absent field of g + o + gl + ep + mu + q + H_2O ± pa. Whether or not the inferred *P–T* path crossed the paragonite fields is unknown, because effective bulk rock composition may have been changed during the retrogression. Anyhow, we suggest the initial retrograde *P–T* evolution to follow an isothermal decompression process, similar to that proposed by Wei et al. (2010) for eclogite at Xinxian. Combined lawsonite-out boundary with isopleths of Si in phengite from the matrix and from composite inclusions in garnet, we interpret the *P–T* regime of 19–20 kbar and 550C–560°C to represent the likely *P–T* conditions for the early retrograde stage. During initial exhumation, in the phase assemblage field of g + o + gl + law + mu + q + H_2O, H_2O content in the bulk composition saturating relevant minerals changed little from 25 to 20 kbar (Figure 8B). On the other hand, when passing through the field g + o + gl + law + ep + mu + H_2O+ q, lawsonite transformed to epidote *via* the reaction law + o → ep + gl ± pa + H_2O and released a large

amount of water. Almost half-weight percent H_2O was released at this process from 20 to 19 kbar (Figure 8B).

Later retrogression led to the replacement of glaucophane by amphibole, omphacite by symplectitic amp + pl ± cpx, garnet by amp + pl corona, phengite by paragonite and paragonite by albite, indicating epidote-amphibolite facies overprint. In the modeled phase diagrams (Figure6D; Figure 7D), the later retrograde *P–T* path successively passed through the phase assemblage fields of g + o + gl + ep + mu + q + H_2O ± pa, g + o + ep + hb + mu + q + pa + H_2O and g + o + ep + hb + mu + q + pl + H_2O. However, this process roughly followed a H_2O increase tendency (Figure 8B). Traditionally viewpoint would expect a fluid-deficient circumstance for the rock system to preserve the mineral assemblage with minimum H_2O content (Guiraud et al., 2001). Therefore, widespread epidote-amphibolite facies overprint in the matrix minerals may imply external fluid infiltration to rock system during late-stage retrogression.

6.2 Factors affecting lawsonite development in continental subduction zones

Studies on natural lawsonite-bearing blueschist and eclogite show that formation of lawsonite requires cold subduction into mantle depths (Tsujimori et al., 2006; Tsujimori and Ernst, 2014). Experimental studies and thermodynamic modeling using a representative MORB composition have shown that under H_2O-saturated conditions, subduction along a geothermal gradient of <8°C/km (which is common in many classic continental subduction zones) would form (U)HP/LT metamorphic rocks in lawsonite stability field (e.g., Okamoto and Maruyama, 1999; Wei, 2011; Tsujimori and Ernst, 2014). Therefore, we can conclude that lawsonite would be expected to form during continental subduction under the assumption of cold and fluid-present conditions. Such a conclusion has been evidenced by pseudomorphs interpreted to be after lawsonite and geochemistry studies (Li et al., 2005; Wei et al., 2010; Guo et al., 2013). However, the problem is, although compiled *P–T* estimates for natural (U)HP metamorphic rocks in continental subduction/collisional orogenic belts fall in lawsonite stability field (Penniston-Dorland et al., 2015), no lawsonite grain has been reported in these rocks. Then, what factors affect the formation and stability of lawsonite during continental subduction and exhumation?

6.2.1 Influence of whole rock composition

The first thing to be considered is fluid (here refers to water) availability during continental subduction since lawsonite is a simple water-rich mineral. A traditional view is that compared to oceanic subduction zones, continental subduction zones are relatively old, dry and cold, with high viscosity, low water availability and low density, thus leading to weak fluid activity during subduction (Zheng et al., 2003; Ernst et al., 2007). In recent years, however, numerous studies have found that a significant amount of H_2O (or hydroxyl) can be stored in various hydrous minerals (e.g., amphibole, phengite, lawsonite, epidote and talc) or nominally anhydrous minerals (e.g., garnet, omphacite, quartz/coesite and kyanite) in continental subduction zones (e.g., Kessel et al., 2005; Hermann et al., 2006; Zheng et al., 2011). In many classic continental subduction-collisional orogenic belt, such as the Alpine, the Himalaya and the Sulu–Dabie, studies on fluid activity during continental subduction include but not limited to dominant and recessive water-bearing components in HP–UHP rocks, rich veins in HP–UHP terrains, abundant water-bearing minerals formed by eclogite retrogression, and polyphase solid inclusions representing the presence of melt/fluid in eclogite minerals (Liou et al., 1998; 2009; 2014; Xiao et al., 2000; Franz et al., 2001; Fu et al., 2002; 2003; Spandler and Hermann, 2006; Zhang Z. et al., 2007; 2008; Zheng and Hermann, 2014). Therefore, in continental subduction zones, it may be really lack fluid activity, but might be rich in some conditions (Chopin, 2003; Bebout, 2007; Beaumont et al., 2009; Zheng, 2009; 2012; Zhao et al., 2015; 2021).

In this study, for the eclogites at Gaoqiao, abundant hydrous minerals were identified as inclusions in garnet showing distinct growth zoning, implying water presence during prograde metamorphic evolution. Besides, as an equivalent to the eclogites, low-grade blueschist and greenschist in the Mulanshan unit suggest water present conditions in shallow subduction zones. These rocks would release free water *via* dehydration reactions to form eclogite when subduction continuously proceeded. To quantify the influence of water content on the formation of lawsonite, we have calculated *P/T*–H_2O phase diagrams (Supplementary Figure S1). Our modeling shows that, in the phase assemblage fields with H_2O > 0.036 wt%, lawsonite is stable under >400°C at 25 kbar or >19 kbar at 550°C. Under H_2O unsaturation conditions (<1.152 wt% at 25 kbar, 550°C; Supplementary Figure S1), the amount of lawsonite is correlated to H_2O content in the bulk rock composition. For instances, lawsonite decreases from 13 to 0 mode% when H_2O content decreases from 1.152 to 0.036 wt% (Supplementary Figure S1). Previous studies have shown that, in (U)HP eclogite, a significant amount of water could be incorporated as both structural OH and molecular H_2O in nominally anhydrous minerals (e.g., Kessel et al., 2005; Hermann et al., 2006; Zheng et al., 2011). For instance, for eclogite in Sulu–Dabie, the total H_2O content including fluid inclusions, hydrous mineral inclusions and structural hydroxyl could be up to 1170–20745 ppm in omphacite and 522–1584 ppm in garnet (Chen et al., 2007). In combination with H_2O retained in some hydrous minerals (e.g., glaucophane, phengite, talc, epidote), we can conclude that for eclogite in western Dabie formed at *P–T* conditions of 25 kbar, 550°C, water content should be sufficient for the formation of lawsonite.

For O and other oxides (MgO, CaO, Na_2O and Al_2O_3) in the bulk rock composition, their influence factors on the formation of lawsonite have also been discussed using *P/T–X* pseudosections (Supplementary Figures S2–S6). The results show that, lawsonite stability field changes little relative to O and X_{MgO} variations (Supplementary Figures S2, 3). On the other hand, X_{Al2O3}, X_{Na2O} and X_{CaO} in the bulk composition may control lawsonite stability field to some extent. For instance, in the *T*–X_{CaO} phase diagram at 25 kbar, lawsonite stability field increases when X_{CaO} increases at X_{CaO} <0.36 (Supplementary Figure S4A); in the *T*–X_{Na2O} phase diagram calculated at 25 kbar, lawsonite stability field varies distinctly at X_{N2O} = 0.1–0.5 and in the *P*–X_{Na2O} phase diagram calculated at 550°C, lawsonite is absent at X_{Na2O} >0.44 (Supplementary Figure S4B); in the *T*–X_{Al2O3} phase diagram calculated at 25 kbar, lawsonite varies distinctly at X_{Al2O3} = 0.3–0.61 and in the *P*–X_{Al2O3} phase diagram calculated at 550°C,

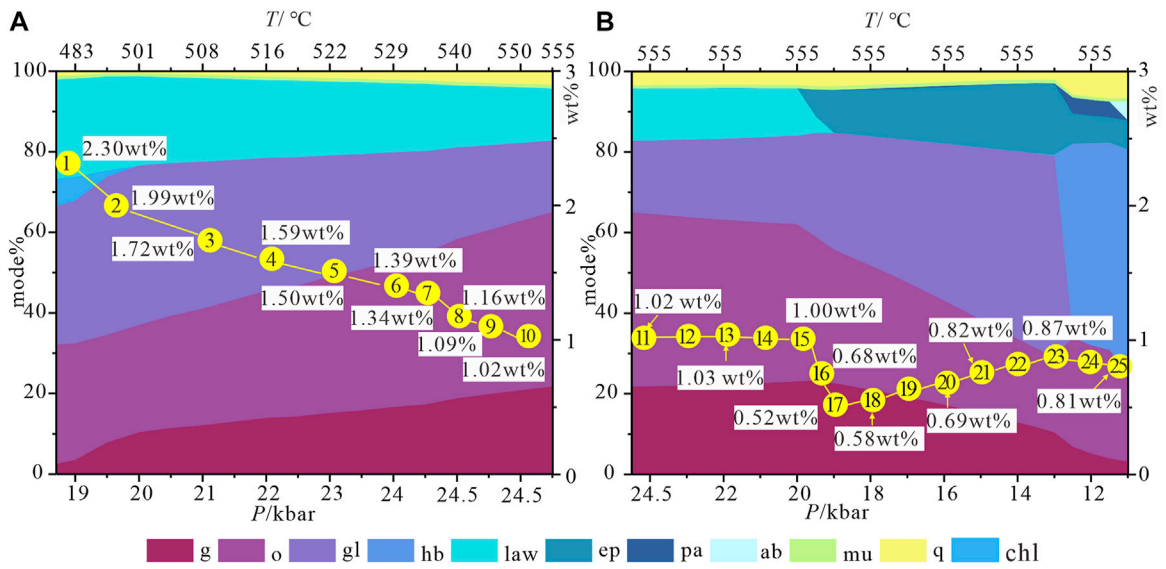

FIGURE 8
Modal variations for different phases (mode%) and corresponding H_2O content (wt%) saturated for relevant assemblages from g + o + gl + chl + law + q + mu **(A)** to g + o + ep + hb + pa + pl + q + mu **(B)** along the inferred *P–T* path in Figure 6.

lawsonite is absent at X_{Al2O3} <0.50. Besides, whole rock compositions of natural intracontinental plate basalts from the GEOROC database (Wang et al., 2016, Supplementary Table S2) and representative natural lawsonite eclogite in the world (Wei, 2011, Supplementary Table S3) were collected and plotted in Supplementary Figures S3–S6. The results show that within those compositional ranges, O and other oxides in the bulk rock composition have little influence on lawsonite development at p = 25 kbar and T = 550°C. However, calculated lawsonite modal variations at 25 kbar, 550°C with increasing X_{MgO}, X_{Al2O3}, X_{Na2O} and X_{CaO} in the whole rock composition show that high X_{MgO} and X_{Al2O3} facilitate more lawsonite formed (Supplementary Figure S8).

6.2.2 Influence of *P–T* evolution

Experimental studies show that lawsonite could be stable at T <830°C with maximum P of 80–90 kbar (Okamoto and Maruyama, 1999), similar to that (T < 760°C and p < 80 kbar) calculated using phase equilibrium modeling using whole-rock composition of the eclogite GQ–2 at Gaoqiao. Therefore, the preservation of lawsonite requires peak temperature during metamorphic evolution to not exceed its thermal stability. When T exceeds the up-temperature of lawsonite stability field, lawsonite may break down to form kyanite *via* the reaction law → ky + czo/ep + q + H_2O or to form ep/czo *via* the reaction law + jd → o + g + czo/ep + H_2O (Wei et al., 2010; Tsuchiya and Hirajima, 2013; Tsujimori and Ernst, 2014; Ren et al., 2018).

Another crucial factor influencing the preservation of lawsonite is retrograde evolution process during exhumation (Wei, 2011; Fedele et al., 2018). In general, two patterns of exhumation *P–T* path may facilitate lawsonite preservation. One is refrigerated exhumation characterized by either hairpin-like (e.g., Ernst, 1988; Vitale Brovarone et al., 2011) or counterclockwise (e.g., Tsujimori and Ernst, 2014; Hunziker et al., 2017) *P–T* path. Substantial cooling during retrogression allows the retrograde evolution across lawsonite stability field and allows the preservation of lawsonite both in the matrix or as inclusions in porphyroblastic minerals (Tsujimori and Ernst, 2014). Another is isothermal decompression characterized by fast exhumation that lawsonite could be preserved only as inclusions in refractory minerals (e.g., garnet, pyrite; Li et al., 2013; Xia et al., 2020), or in a specific condition, in the matrix as has been reported for lawsonite-bearing eclogite xenoliths in kimberlitic pipes from Colorado Plateau (Usui et al., 2006). Isothermal decompression may lead to retrograde *P–T* path across lawsonite-epidote transition curve and thus to breakdown of lawsonite. The breakdown of lawsonite could release a significant amount of H_2O, causing retrogression and forming polymineralic aggregates showing pseudomorphs of lawsonite (Wei, 2011; Tian and Wei, 2013; Xia et al., 2020). In this study, by combining petrographic studies and phase equilibrium modeling, we show the retrograde *P–T* path for the eclogites at Gaoqiao to follow an isothermal decompression process. Therefore, the breakdown of lawsonite may be due to the isothermal exhumation.

6.3 luid behavior during lawsonite breakdown

As mentioned above, previous studies have proved intense fluid activity in continental subduction zones. During subduction, our phase equilibrium modelling for the eclogites at Gaoqiao (Figure 6B; Figure 7B) shows that the modal contents of hydrous minerals (e.g., chlorite, lawsonite and glaucophane) gradually decreased to form anhydrous minerals (e.g., garnet and omphacite) along the progressive *P–T* evolution (Figure 8A). The

modeled reactions are o + chl → g + gl + law + H_2O at low temperature (<501°C) and gl + law → g + o + H_2O at high temperature (>501°C). Figure 8A shows that, during this process, water content in the bulk composition to be saturated relevant hydrous minerals decreased from 2.30 to 1.02 wt% (Point 1–10).

Subsequent ITD exhumation led the *P–T* path to cross lawsonite-epidote transition fields (Figure 6D; Figure 7D). However, detailed mechanism for lawsonite breakdown is still unknown. On one hand, Hamelin et al. (2018) proposed that lawsonite breakdown must be in part driven by reaction of lawsonite with the celadonite content of phengitic mica in the matrix, to form celadonite-poor phengite in the pseudomorphs. Phengite should become less rich in celadonite with an increase in temperature to drive lawsonite breakdown. On the other hand, the breakdown of lawsonite may only be driven by pressure decrease to cross the H_2O-decrease isopleths during exhumation (Wei, 2011). Under this assumption, phengite with lower celadonite in pseudomorphs could be formed from K-bearing fluid at relatively lower pressure when lawsonite transformed to epidote.

Our phase diagrams show that, the breakdown of lawsonite released almost ~50% of H_2O in the bulk rock composition (from 1.02 to 0.52 wt%) (Point 15 to 17 in Figure 8B). Based on petrographic observation and mineral chemistry, we infer a range of elements migrated with fluid to form various types of polyphase pseudomorphs after lawsonite. For type 1 pseudomorphs with mineral aggregates of czo/ep + pa/ab ± q (Figures 5A–D), the balanced reaction 1 implies additional Na^+ and/or Si^{4+} to the original lawsonite. For type 2 pseudomorphs with amp-bearing mineral aggregates of czo + pa/ab + amp (Figures 5E–H), except for added Na^+ and lost water, Fe/Mg should be introduced by fluid (reactions two and 3). Omphacite may participate in this process. For type 3 pseudomorphs with largely phengite, paragonite/albie and rare czo/ep (Figures 5I,K), K^+ and Na^+ should be introduced by fluid ingress and Ca^{2+} must have been lost to form amphibole or epidote in the matrix by fluid egress. For type 4 pseudomorphs dominated by quartz and/or phengite, Ca^{2+} and/or Al^{3+} must be lost while Si and/or K should be introduced by fluid ingress (Figures 5J, L). Tiny fractures around these polymineralic inclusions are interpreted to provide pathways for fluid activity.

Accordingly, the mechanism causing lawsonite breakdown during continental subduction and exhumation may be due to the change of *P-T* conditions and fluid environments, which promote the lawsonite of lawsonite by reaction with surrounding minerals. In addition, phase equilibrium modelling suggests that during continental plate subduction, lawsonite can absorb the water that was released from water-bearing minerals during the initial stages of subduction (e.g., chlorite, chlorite, hornblende, *etc.*) and carry it into the deeper parts of the subduction zone. In cold geothermal gradient subduction zones, it can even carry water into the mantle to release, causing partial melting and facilitating crust-mantle interactions (Zheng, 2009; Zheng et al., 2011). During the exhumation process, the lawsonite breakdown and releases abundant water due to the change of *P-T* conditions, resulting in the formation of metamorphic veins in (U)HP eclogites and the growth of new minerals, and causing local element migration or metasomatism (Li et al., 2005; Herman et al., 2006; Chen et al., 2007; Guo et al., 2013; Zheng and Hermann, 2014). And the fluid released during the deep subduction exhumation process can accumulate locally, and may even cause the overlying rock to dehydrate and melt to form syn-exhumation magma (Miller et al., 2002; Zheng, 2009; Zhao et al., 2015).

7 Conclusion

(1) Abundant polymineralic aggregates of epidote/clinozoisite + paragonite/albite ± other minerals showing distinct rectangular or rhombic shapes developed as inclusions in garnet or in the matrix from the eclogites at Gaoqiao, western Dabie. Recalculated bulk composition of the composite pseudomorphs is similar to that of ideal lawsonite. Therefore, we interpret the composite mineral aggregates as pseudomorphs after lawsonite.

(2) Based on petrology and phase equilibrium modelling, a convex *P–T* path has been inferred for the eclogites at Gaoqiao, western Dabie.

(3) We have quantified the influence of bulk rock composition on the development of lawsonite during continental subduction using a series of *P/T–X* pseudosections. The results show that, H_2O content in the bulk rock composition is the most important factor, whereas O (Fe^{3+}), X_{MgO} [MgO/(MgO+FeO)], XCaO [CaO/(CaO+MgO+FeO+MnO+Na2O)], XNa2O [(Na2O/(CaO+Na2O)] and XAl2O3 [Al2O3/(Al_2O_3+CaO+Na_2O)] in bulk rock compositions have only slight or no influence on lawsonite appearance.

(4) During continent subduction along low geothermal gradient (5°C–8°C/km), lawsonite can be formed under H_2O present conditions. The absence of lawsonite in natural eclogite may be ascribed to retrograde overprint during exhumation.

Data availability statement

The original contributions presented in the study are included in the article/Supplementary Material. further inquiries can be directed to the corresponding authors.

Author contributions

XL and BX wrote the manuscript. BX and QY designed and funded the project. YW revised the manuscript and funded the project.

Funding

This study was financially supported by the National Natural Science Foundation of China (42130307 and 41625008).

Acknowledgments

We thank the Guest Associate Editor Yi-Xiang Chen, reviewer Songjie Wang and two reviewers to reviewers Songjie Wang, Ren-Xu Chen and Tatsuki Tsujimori.

Conflict of interest

The authors declare that the research was conducted in the absence of any commercial or financial relationships that could be construed as a potential conflict of interest.

Publisher's note

All claims expressed in this article are solely those of the authors and do not necessarily represent those of their affiliated organizations, or those of the publisher, the editors and the reviewers. Any product that may be evaluated in this article, or claim that may be made by its manufacturer, is not guaranteed or endorsed by the publisher.

Supplementary material

The Supplementary Material for this article can be found online at: https://www.frontiersin.org/articles/10.3389/feart.2023.1138170/full#supplementary-material

References

Angiboust, S., and Agard, P. (2010). Initial water budget: The key to detaching large volumes of eclogitized oceanic crust along the subduction channel? *Lithos* 120, 453–474. doi:10.1016/j.lithos.2010.09.007

Angiboust, S., Langdon, R., Agard, P., Waters, D., and Chopin, C. (2012). Eclogitization of the Monviso ophiolite (W. Alps) and implications on subduction dynamics. *J. Metamorph. Geol.* 30, 37–61. doi:10.1111/j.1525-1314.2011.00951.x

Barnicoat, A. C., and Fry, N. (1986). High-pressure metamorphism of the Zermatt-Saas ophiolite zone, Switzerland. *J. Geol. Soc.* 143, 607–618. doi:10.1144/gsjgs.143.4.0607

Beaumont, C., Jamieson, R. A., Butler, J. P., and Warren, C. J. (2009). Crustal structure: A key constraint on the mechanism of ultra-high-pressure rock exhumation. *Earth Planet. Sci. Lett.* 287, 116–129. doi:10.1016/j.epsl.2009.08.001

Bebout, G. E. (2007). Metamorphic chemical geodynamics of subduction zones. *Earth Planet. Sci. Lett.* 260, 373–393. doi:10.1016/j.epsl.2007.05.050

Castelli, D., Rolfo, F., Compagnoni, R., and Xu, S. (1998). Metamorphic veins with kyanite, zoisite and quartz in the Zhu-Jia-Chong eclogite, Dabie Shan, China. *Isl. Arc.* 7, 159–173. doi:10.1046/j.1440-1738.1998.00185.x

Chen, R., Zheng, Y., Gong, B., Zhao, Z., Gao, T., Chen, B., et al. (2007). Origin of retrograde fluid in ultrahigh-pressure metamorphic rocks: Constraints from mineral hydrogen isotope and water content changes in eclogite-gneiss transitions in the Sulu orogen. *Geochim. Cosmochim. Acta* 71, 2299–2325. doi:10.1016/j.gca.2007.02.012

Cheng, H., and Cao, D. (2015). Protracted garnet growth in high-P eclogite: Constraints from multiple geochronology and P-T pseudosection. *J. Metamorph. Geol.* 33, 613–632. doi:10.1111/jmg.12136

Cheng, H., DuFrane, S. A., Vervoort, J. D., Nakamura, E., Li, Q., and Zhou, Z. (2010). The Triassic age for oceanic eclogites in the Dabie orogen: Entrainment of oceanic fragments in the continental subduction. *Lithos* 117, 82–98. doi:10.1016/j.lithos.2010.02.007

Cheng, H., King, R. L., Nakamura, E., Vervoort, J. D., Zheng, Y., Ota, T., et al. (2009). Transitional time of oceanic to continental subduction in the Dabie orogen: Constraints from U-Pb, Lu-Hf, Sm-Nd and Ar-Ar multichronometric dating. *Lithos* 110, 327–342. doi:10.1016/j.lithos.2009.01.013

Chopin, C. (2003). Ultrahigh-pressure metamorphism: Tracing continental crust into the mantle. *Earth Planet. Sci. Lett.* 212, 1–14. doi:10.1016/s0012-821x(03)00261-9

Coggon, R., and Holland, T. (2002). Mixing properties of phengitic micas and revised garnet-phengite thermobarometers. *J. Metamorph. Geol.* 20, 683–696. doi:10.1046/j.1525-1314.2002.00395.x

Diener, J., and Powell, R. (2012). Revised activity-composition models for clinopyroxene and amphibole. *J. Metamorph. Geol.* 30, 131–142. doi:10.1111/j.1525-1314.2011.00959.x

Du, J. X., Zhang, L. F., Bader, T., Chen, Z. Y., and Lü, Z. (2014). Metamorphic evolution of relict lawsonite-bearing eclogites from the (U) HP metamorphic belt in the Chinese southwestern Tianshan. *J. Metamorph. Geol.* 32, 575–598. doi:10.1111/jmg.12080

Ernst, W. G. (1988). Tectonic history of subduction zones inferred from retrograde blueschist PT paths. *Geology* 16, 1081–1084. doi:10.1130/0091-7613(1988)016<1081:thoszi>2.3.co;2

Ernst, W. G., Tsujimori, T., Zhang, R., and Liou, J. G. (2007). Permo-Triassic collision, subduction-zone metamorphism, and tectonic exhumation along the East Asian continental margin. *Annu. Rev. Earth Planet. Sci.* 35, 73–110. doi:10.1146/annurev.earth.35.031306.140146

Evans, T. P. (2004). A method for calculating effective bulk composition modification due to crystal fractionation in garnet-bearing schist: Implications for isopleth thermobarometry: Garnet fractionation and P-T path calculation. *J. Metamorph. Geol.* 22, 547–557. doi:10.1111/j.1525-1314.2004.00532.x

Fedele, L., Tramparulo, F. D., Vitale, S., Cappelletti, P., Prinzi, E. P., and Mazzoli, S. (2018). Petrogenesis and deformation history of the lawsonite-bearing blueschist facies metabasalts of the Diamante-Terranova oceanic unit (southern Italy). *J. Metamorph. Geol.* 36, 691–714. doi:10.1111/jmg.12303

Franz, L., Romer, R. L., Klemd, R., Schmid, R., Oberhansli, R., Wagner, T., et al. (2001). Eclogite-facies quartz veins within metabasites of the Dabie Shan (eastern China): Pressure-temperature-time-deformation path, composition of the fluid phase and fluid flow during exhumation of high-pressure rocks. *Contrib. Mineral. Petrol.* 141, 322–346. doi:10.1007/s004100000233

Fu, B., Touret, J. L., Zheng, Y., and Jahn, B. (2003). Fluid inclusions in granulites, granulitized eclogites and garnet clinopyroxenites from the Dabie-Sulu terranes, eastern China. *Lithos* 70, 293–319. doi:10.1016/s0024-4937(03)00103-8

Fu, B., Zheng, Y., and Touret, J. L. (2002). Petrological, isotopic and fluid inclusion studies of eclogites from Sujiahe, NW Dabie Shan (China). *Chem. Geol.* 187, 107–128. doi:10.1016/s0009-2541(02)00014-1

Godard, G. (2010). Two orogenic cycles recorded in eclogite-facies gneiss from the southern Armorican Massif (France). *Eur. J. Mineral.* 21, 1173–1190. doi:10.1127/0935-1221/2009/0021-1984

Green, E., Holland, T., and Powell, R. (2007). An order-disorder model for omphacitic pyroxenes in the system jadeite-diopside-hedenbergite-acmite, with applications to eclogitic rocks. *Am. Min.* 92, 1181–1189. doi:10.2138/am.2007.2401

Guiraud, M., Powell, R., and Rebay, G. (2001). H2O in metamorphism and unexpected behaviour in the preservation of metamorphic mineral assemblages. *J. Metamorph. Geol.* 19, 445–454. doi:10.1046/j.0263-4929.2001.00320.x

Guo, S., Ye, K., Wu, T. F., Chen, Y., Yang, Y. H., Zhang, L. M., et al. (2013). A potential method to confirm the previous existence of lawsonite in eclogite: The mass imbalance of Sr and LREE s in multistage epidote (ganghe, Dabie UHP terrane). *J. Metamorph. Geol.* 31, 415–435. doi:10.1111/jmg.12027

Hacker, B. R., Ratschbacher, L., Webb, L., McWilliams, M. O., Ireland, T., Calvert, A., et al. (2000). Exhumation of ultrahigh-pressure continental crust in east central China: Late Triassic-Early Jurassic tectonic unroofing. *J. Geophys. Res. Solid Earth* 105, 13339–13364. doi:10.1029/2000jb900039

Hamelin, C., Brady, J. B., Cheney, J. T., Schumacher, J. C., Able, L. M., and Sperry, A. J. (2018). Pseudomorphs after lawsonite from syros, Greece. *J. Petrol.* 59, 2353–2384. doi:10.1093/petrology/egy099

Hara, T., Tsujimori, T., Chang, Q., and Kimura, J. (2018). *In-situ* Sr-Pb isotope geochemistry of lawsonite: A new method to investigate slab-fluids. *Lithos* 320, 93–104. doi:10.1016/j.lithos.2018.09.001

Hawthorne, F. C., Oberti, R., Harlow, G. E., Maresch, W. V., Martin, R. F., Schumacher, J. C., et al. (2012). Nomenclature of the amphibole supergroup. *Am. Min.* 97, 2031–2048. doi:10.2138/am.2012.4276

Hermann, J., Spandler, C., Hack, A., and Korsakov, A. V. (2006). Aqueous fluids and hydrous melts in high-pressure and ultra-high pressure rocks: Implications for element transfer in subduction zones. *Lithos* 92, 399–417. doi:10.1016/j.lithos.2006.03.055

Holland, T., Baker, J., and Powell, R. (1998). Mixing properties and activity-composition relationships of chlorites in the system MgO-FeO-Al_2O_3-SiO_2-H_2O. *Eur. J. Mineral.* 10, 395–406. doi:10.1127/ejm/10/3/0395

Holland, T., and Powell, R. (2003). Activity-composition relations for phases in petrological calculations: An asymmetric multicomponent formulation. *Contrib. Mineral. Petrol.* 145, 492–501. doi:10.1007/s00410-003-0464-z

Holland, T., and Powell, R. (2011). An improved and extended internally consistent thermodynamic dataset for phases of petrological interest, involving a new equation of state for solids. *J. Metamorph. Geol.* 29, 333–383. doi:10.1111/j.1525-1314.2010.00923.x

Holland, T., and Powell, R. (1998). An internally consistent thermodynamic data set for phases of petrological interest. *J. Metamorph. Geol.* 16, 309–343. doi:10.1111/j.1525-1314.1998.00140.x

Hunziker, D., Burg, J. P., Moulas, E., Reusser, E., and Omrani, J. (2017). formation and preservation of fresh lawsonite: Geothermobarometry of the North makran blueschists, southeast Iran. *J. Metamorph. Geol.* 35, 871–895. doi:10.1111/jmg.12259

Jahn, B., Liu, X., Yui, T., Morin, N., and Coz, M. B. (2005). High-pressure/ultrahigh-pressure eclogites from the hong'an block, east-central China: Geochemical characterization, isotope disequilibrium and geochronological controversy. *Contrib. Mineral. Petrol.* 149, 499–526. doi:10.1007/s00410-005-0668-5

Kessel, R., Schmidt, M. W., Ulmer, P., and Pettke, T. (2005). Trace element signature of subduction-zone fluids, melts and supercritical liquids at 120-180 km depth. *Nature* 437, 724–727. doi:10.1038/nature03971

Li, J., Gao, J., John, T., Klemd, R., and Su, W. (2013). Fluid-mediated metal transport in subduction zones and its link to arc-related giant ore deposits: Constraints from a sulfide-bearing HP vein in lawsonite eclogite (Tianshan, China). *Geochim. Cosmochim. Acta* 120, 326–362. doi:10.1016/j.gca.2013.06.023

Li, X., Li, Y., and Shu, G. (2005). Breakdown of lawsonite subsequent to peak UHP metamorphism in the Dabie terrane and its implication for fluid activity. *Chin. Sci. Bull.* 50, 1366–1372. doi:10.1360/982004-407

Li, X., Zheng, Y., Wu, Y., Chen, F., Gong, B., and Li, Y. (2004). Low-T eclogite in the Dabie terrane of China: Petrological and isotopic constraints on fluid activity and radiometric dating. *Contrib. Mineral. Petrol.* 148, 443–470. doi:10.1007/s00410-004-0616-9

Liou, J. G., Ernst, W. G., Zhang, R. Y., Tsujimori, T., and Jahn, B. M. (2009). Ultrahigh-pressure minerals and metamorphic terranes–the view from China. *J. Asian Earth Sci.* 35, 199–231. doi:10.1016/j.jseaes.2008.10.012

Liou, J. G., Tsujimori, T., Yang, J., Zhang, R. Y., and Ernst, W. G. (2014). Recycling of crustal materials through study of ultrahigh-pressure minerals in collisional orogens, ophiolites, and mantle xenoliths: A review. *J. Asian Earth Sci.* 96, 386–420. doi:10.1016/j.jseaes.2014.09.011

Liou, J. G., Zhang, R. Y., Ernst, W. G., Rumble, D., and Maruyama, S. (1998). High-pressure minerals from deeply subducted metamorphic rocks. *Rev. Mineralogy Geochem.* 37, 33–96.

Liu, J., Ye, K., and Sun, M. (2006). Exhumation P-T path of UHP eclogites in the hong'an area, Western Dabie mountains, China. *Lithos* 89, 154–173. doi:10.1016/j.lithos.2005.12.002

Liu, Q., Hermann, J., and Zhang, J. (2013). Polyphase inclusions in the Shuanghe UHP eclogites formed by subsolidus transformation and incipient melting during exhumation of deeply subducted crust. *Lithos* 177, 91–109. doi:10.1016/j.lithos.2013.06.010

Liu, X. C., Wu, Y. B., Gao, S., Wang, J., Peng, M., Gong, H. J., et al. (2011). Zircon U-Pb and Hf evidence for coupled subduction of oceanic and continental crust during the Carboniferous in the Huwan shear zone, Western Dabie orogen, central China. *J. Metamorph. Geol.* 29, 233–249. doi:10.1111/j.1525-1314.2010.00914.x

Liu, X., Jahn, B., Liu, D., Dong, S., and Li, S. (2004). SHRIMP U-Pb zircon dating of a metagabbro and eclogites from Western Dabieshan (Hong'an Block), China, and its tectonic implications. *Tectonophysics* 394, 171–192. doi:10.1016/j.tecto.2004.08.004

Liu, X., Wei, C., Li, S., Dong, S., and Liu, J. (2004). Thermobaric structure of a traverse across Western dabieshan: Implications for collision tectonics between the sino-Korean and yangtze cratons. *J. Metamorph. Geol.* 22, 361–379. doi:10.1111/j.1525-1314.2004.00519.x

Lou, Y., Wei, C., Liu, X., Zhang, C., Tian, Z., and Wang, W. (2013). Metamorphic evolution of garnet amphibolite in the Western Dabieshan eclogite belt, Central China: Evidence from petrography and phase equilibria modeling. *J. Asian Earth Sci.* 63, 130–138. doi:10.1016/j.jseaes.2012.11.031

Lü, Z., Zhang, L., Yue, J., and Li, X. (2019). Ultrahigh-pressure and high-P lawsonite eclogites in Muzhaerte, Chinese Western Tianshan. *J. Metamorph. Geol.* 37, jmg.12482–743. doi:10.1111/jmg.12482

Martin, L., Hermann, J., Gauthiez Putallaz, L., Whitney, D. L., Vitale Brovarone, A., Fornash, K. F., et al. (2014). Lawsonite geochemistry and stability–implication for trace element and water cycles in subduction zones. *J. Metamorph. Geol.* 32, 455–478. doi:10.1111/jmg.12093

Mattinson, C. G., Wooden, J. L., Liou, J. G., Bird, D. K., and Wu, C. L. (2006). Age and duration of eclogite-facies metamorphism, North Qaidam HP/UHP terrane, Western China. *Am. J. Sci.* 306, 683–711. doi:10.2475/09.2006.01

Miller, J. A., Buick, I. S., Cartwright, I., Barnicoat, A., Cuthbert, S. J., and Ballevre, M. (2002). Fluid processes during the exhumation of high-P metamorphic belts. *Mineral. Mag.* 66, 93–119. doi:10.1180/0026461026610016

Morimoto, N. (1988). Nomenclature of pyroxenes. *Mineral. Petrol.* 39, 55–76. doi:10.1007/bf01226262

Okamoto, K., and Maruyama, S. (1999). The high-pressure synthesis of lawsonite in the MORB+ H2O system. *Am. Min.* 84, 362–373. doi:10.2138/am-1999-0320

Orozbaev, R., Hirajima, T., Bakirov, A., Takasu, A., Maki, K., Yoshida, K., et al. (2015). Trace element characteristics of clinozoisite pseudomorphs after lawsonite in talc-garnet-chloritoid schists from the Makbal UHP Complex, northern Kyrgyz Tian-Shan. *Lithos* 226, 98–115. doi:10.1016/j.lithos.2014.10.008

Penniston-Dorland, S. C., Kohn, M. J., and Manning, C. E. (2015). The global range of subduction zone thermal structures from exhumed blueschists and eclogites: Rocks are hotter than models. *Earth Planet. Sci. Lett.* 428, 243–254. doi:10.1016/j.epsl.2015.07.031

Pognante, U. (1989). Tectonic implications of lawsonite formation in the Sesia zone (Western Alps). *Tectonophysics* 162, 219–227. doi:10.1016/0040-1951(89)90245-x

Poli, S., and Schmidt, M. W. (1995). H2O transport and release in subduction zones: Experimental constraints on basaltic and andesitic systems. *J. Geophys. Res. Solid Earth* 100, 22299–22314. doi:10.1029/95jb01570

Powell, R., Holland, T., and Worley, B. (1998). Calculating phase diagrams involving solid solutions via non-linear equations, with examples using THERMOCALC. *J. Metamorph. Geol.* 16, 577–588. doi:10.1111/j.1525-1314.1998.00157.x

Ratschbacher, L., Franz, L., Enkelmann, E., Jonckheere, R., Pörschke, A., Hacker, B. R., et al. (2006). The Sino-Korean-Yangtze suture, the Huwan detachment, and the Paleozoic-Tertiary exhumation of (ultra) high-pressure rocks along the Tongbai-Xinxian-Dabie Mountains. *Special Papers-Geological Soc. Am.* 403, 45.

Ren, Y. F., Chen, D. L., Kelsey, D. E., Gong, X. K., Liu, L., Zhu, X. H., et al. (2018). Metamorphic evolution of a newly identified Mesoproterozoic oceanic slice in the Yuka terrane and its implications for a multi-cyclic orogenic history of the North Qaidam UHPM belt. *J. Metamorph. Geol.* 36, 463–488. doi:10.1111/jmg.12300

Reynard, B., and Bass, J. D. (2014). Elasticity of lawsonite and seismological signature of metamorphism and water cycling in the subducting oceanic crust. *J. Metamorph. Geol.* 32, 479–487. doi:10.1111/jmg.12072

Scambelluri, M., and Philippot, P. (2001). Deep fluids in subduction zones. *Lithos* 55, 213–227. doi:10.1016/s0024-4937(00)00046-3

Schmidt, M. W., and Poli, S. (2003). Generation of mobile components during subduction of oceanic crust. *Treatise Geochem.* 3, 659.

Smith, D., and Zientek, M. (1979). Mineral chemistry and zoning in eclogite inclusions from Colorado Plateau diatremes. *Contrib. Mineral. Petrol.* 69, 119–131. doi:10.1007/bf00371855

Spandler, C., Hermann, J., Arculus, R., and Mavrogenes, J. (2003). Redistribution of trace elements during prograde metamorphism from lawsonite blueschist to eclogite facies; implications for deep subduction-zone processes. *Contrib. Mineral. Petrol.* 146, 205–222. doi:10.1007/s00410-003-0495-5

Spandler, C., and Hermann, J. (2006). High-pressure veins in eclogite from New Caledonia and their significance for fluid migration in subduction zones. *Lithos* 89, 135–153. doi:10.1016/j.lithos.2005.12.003

Spear, F. S. (1993). *Metamorphic phase equilibria and pressure-temperature-time paths*. Washington, DC: Mineralogical Society of America Monograph, 352–356.

Tatsumi, Y., and Kogiso, T. (2003). The subduction factory: Its role in the evolution of the earth's crust and mantle. *Geol. Soc. Lond. Spec. Publ.* 219, 55–80. doi:10.1144/gsl.sp.2003.219.01.03

Tatsumi, Y. (1989). Migration of fluid phases and Genesis of basalt magmas in subduction zones. *J. Geophys. Res. Solid Earth* 94, 4697–4707. doi:10.1029/jb094ib04p04697

Tian, Z. L., and Wei, C. J. (2013). Metamorphism of ultrahigh-pressure eclogites from the kebuerte valley, south tianshan, NW China: Phase equilibria andP-T path. *J. Metamorph. Geol.* 31, 281–300. doi:10.1111/jmg.12021

Tsuchiya, S., and Hirajima, T. (2013). Evidence of the lawsonite eclogite facies metamorphism from an epidote-glaucophane eclogite in the Kotsu area of the Sanbagawa belt, Japan. *J. Mineral. Petrol. Sci.* 108, 166–171. doi:10.2465/jmps.121022b

Tsujimori, T., and Ernst, W. G. (2014). Lawsonite blueschists and lawsonite eclogites as proxies for palaeo-subduction zone processes: A review. *J. Metamorph. Geol.* 32, 437–454. doi:10.1111/jmg.12057

Tsujimori, T., Sisson, V., Liou, J., Harlow, G., and Sorensen, S. (2006). Very-low-temperature record of the subduction process: A review of worldwide lawsonite eclogites. *Lithos* 92, 609–624. doi:10.1016/j.lithos.2006.03.054

Usui, T., Nakamura, E., and Helmstaedt, H. (2006). Petrology and geochemistry of eclogite xenoliths from the Colorado plateau: Implications for the evolution of subducted oceanic crust. *J. Petrol.* 47, 929–964. doi:10.1093/petrology/egi101

Vitale Brovarone, A., Alard, O., Beyssac, O., Martin, L., and Picatto, M. (2014). Lawsonite metasomatism and trace element recycling in subduction zones. *J. Metamorph. Geol.* 32, 489–514. doi:10.1111/jmg.12074

Vitale Brovarone, A., Groppo, C., Hetényi, G., Compagnoni, R., and Malavieille, J. (2011). Coexistence of lawsonite-bearing eclogite and blueschist: Phase equilibria modelling of alpine corsica metabasalts and petrological evolution of subducting slabs. *J. Metamorph. Geol.* 29, 583–600. doi:10.1111/j.1525-1314.2011.00931.x

Wang, J, R., Pan, Z, J., Zhang, Q., Chen, W, F., Yang, J., Jiao, S, T., et al. (2016). Intra-continental basalt data mining: The diversity of their constituents and the performance in basalt discrimination diagrams. *Acta Petrol. Sin.* 32, 1919–1933.

Wei, C. J. (2011). Calculated phase equilibria for MORB compositions: A reappraisal of the metamorphic evolution of lawsonite eclogite. *J. Metamorph. Geol.* 29, 939–952. doi:10.1111/j.1525-1314.2011.00948.x

Wei, C. J., Li, Y. J., Yu, Y., and Zhang, J. S. (2010). Phase equilibria and metamorphic evolution of glaucophane-bearing UHP eclogites from the Western Dabieshan Terrane, Central China. *J. Metamorph. Geol.* 28, 647–666. doi:10.1111/j.1525-1314.2010.00884.x

White, R. W., Pomroy, N. E., and Powell, R. (2005). An *in situ* metatexite-diatexite transition in upper amphibolite facies rocks from Broken Hill, Australia. *J. Metamorph. Geol.* 23, 579–602. doi:10.1111/j.1525-1314.2005.00597.x

Whitney, D. L., and Davis, P. B. (2006). Why is lawsonite eclogite so rare? Metamorphism and preservation of lawsonite eclogite, sivrihisar, Turkey. *Geol. (Boulder)* 34, 473–476. doi:10.1130/G22259.1

Wu, Y., Gao, S., Zhang, H., Yang, S., Jiao, W., Liu, Y., et al. (2008). Timing of UHP metamorphism in the hong'an area, Western Dabie mountains, China: Evidence from zircon U-Pb age, trace element and Hf isotope composition. *Contrib. Mineral. Petrol.* 155, 123–133. doi:10.1007/s00410-007-0231-7

Wu, Y., Hanchar, J. M., Gao, S., Sylvester, P. J., Tubrett, M., Qiu, H., et al. (2009). Age and nature of eclogites in the Huwan shear zone, and the multi-stage evolution of the Qinling-Dabie-Sulu orogen, central China. *Earth Planet. Sci. Lett.* 277, 345–354. doi:10.1016/j.epsl.2008.10.031

Wu, Y., and Zheng, Y. (2013). Tectonic evolution of a composite collision orogen: An overview on the qinling-tongbai-hong'an-dabie-sulu orogenic belt in central China. *Gondwana Res.* 23, 1402–1428. doi:10.1016/j.gr.2012.09.007

Xia, B., Brown, M., and Zhang, L. (2020). P-T evolution and tectonic significance of lawsonite-bearing schists from the eastern segment of the southwestern Tianshan, China. *J. Metamorph. Geol.* 38, 935–962. doi:10.1111/jmg.12555

Xia, B., Cui, Y., Shang, Y. F., and Shi, J. T. (2022b). Petrology of eclogite at huwan, western Dabie and implications for phase equilibrium modeling on LT-HP/UHP eclogite. *J. Earth S. C.* doi:10.1007/s12583-022-1719-9

Xia, B., Shang, Y, F., Lu, X, B., and Wu, Y, B. (2022a). UHP eclogite from Western Dabie records evidence of polycyclic burial during continental subduction. *Am. Mineralogist*. doi:10.2138/am-2022-8446

Xiao, Y., Hoefs, J., van den Kerkhof, A. M., Fiebig, J., and Zheng, Y. (2000). Fluid history of UHP metamorphism in Dabie Shan, China: A fluid inclusion and oxygen isotope study on the coesite-bearing eclogite from bixiling. *Contrib. Mineral. Petrol.* 139, 1–16. doi:10.1007/s004100050570

Zhang, J. X., Meng, F. C., and Wan, Y. S. (2007a). A cold early palaeozoic subduction zone in the North qilian mountains, NW China: Petrological and U-Pb geochronological constraints. *J. Metamorph. Geol.* 25, 285–304. doi:10.1111/j.1525-1314.2006.00689.x

Zhang, R., and Liou, J. G. (1994). Coesite-bearing eclogite in henan province, central China: Detailed petrography, glaucophane stability and PT-path. *Eur. J. Mineral.* 6, 217–234. doi:10.1127/ejm/6/2/0217

Zhang, Z., Shen, K., Liou, J. G., and Zhao, X. (2007b). Fluid inclusions associated with exsolved quartz needles in omphacite of UHP eclogites, Chinese Continental Scientific Drilling Main Drill Hole. *Int. Geol. Rev.* 49, 479–486. doi:10.2747/0020-6814.49.5.479

Zhang, Z., Shen, K., Sun, W., Liu, Y., Liou, J. G., Shi, C., et al. (2008). Fluids in deeply subducted continental crust: Petrology, mineral chemistry and fluid inclusion of UHP metamorphic veins from the Sulu orogen, eastern China. *Geochim. Cosmochim. Acta* 72, 3200–3228. doi:10.1016/j.gca.2008.04.014

Zhao, Z, F., Cheng, R, X., Chen, Y, X., Dai, L, Q., and Zheng, Y, F. (2021). Progresses in the Study of partial melting of ultrahigh-pressure metamorphic rocks and crust-mantle interaction in continental subduction zones. *Bull. Mineralogy, Petrology Geochem.* 40, 36–59.

Zhao, Z, F., Dai, L, Q., and Zheng, Y, F. (2015). Two types of the crust-mantle interaction in continental subduction zones. *Sci. China Earth Sci.* 58, 1269–1283. doi:10.1007/s11430-015-5136-0

Zheng, Y. (2009). Fluid regime in continental subduction zones: Petrological insights from ultrahigh-pressure metamorphic rocks. *J. Geol. Soc.* 166, 763–782. doi:10.1144/0016-76492008-016r

Zheng, Y., Fu, B., Gong, B., and Li, L. (2003). Stable isotope geochemistry of ultrahigh pressure metamorphic rocks from the dabie-sulu orogen in China: Implications for geodynamics and fluid regime. *Earth-Sci. Rev.* 62, 105–161. doi:10.1016/s0012-8252(02)00133-2

Zheng, Y., and Hermann, J. (2014). Geochemistry of continental subduction-zone fluids. *Earth, Planets Space* 66, 93–16. doi:10.1186/1880-5981-66-93

Zheng, Y. (2012). Metamorphic chemical geodynamics in continental subduction zones. *Chem. Geol.* 328, 5–48. doi:10.1016/j.chemgeo.2012.02.005

Zheng, Y. (2008). Research progress of ultrahigh pressure metamorphism and continental collision: A case study of dabie-sulu orogenic belt. *Chin. Sci. Bull.* 53, 2129–2152.

Zheng, Y., Xia, Q., Chen, R., and Gao, X. (2011). Partial melting, fluid supercriticality and element mobility in ultrahigh-pressure metamorphic rocks during continental collision. *Earth-Sci. Rev.* 107, 342–374. doi:10.1016/j.earscirev.2011.04.004

Zhong, Z., Suo, S., and You, Z. (1999). Regional-scale extensional tectonic pattern of ultrahigh-pressure and high-pressure metamorphic belts from the Dabie massif, China. *Int. Geol. Rev.* 41, 1033–1041. doi:10.1080/00206819909465188

Zhong, Z., Suo, S., You, Z., Zhang, H., and Zhou, H. (2001). Major constituents of the Dabie collisional orogenic belt and partial melting in the ultrahigh-pressure unit. *Int. Geol. Rev.* 43, 226–236. doi:10.1080/00206810109465010

Zhou, L., Xia, Q., Zheng, Y., Chen, R., Hu, Z., and Yang, Y. (2015). Tectonic evolution from oceanic subduction to continental collision during the closure of paleotethyan ocean: Geochronological and geochemical constraints from metamorphic rocks in the hong'an orogen. *Gondwana Res.* 28, 348–370. doi:10.1016/j.gr.2014.03.009

Zhou, L., Xia, Q., Zheng, Y., and Hu, Z. (2014). Polyphase growth of garnet in eclogite from the Hong'an orogen: Constraints from garnet zoning and phase equilibrium. *Lithos* 206, 79–99. doi:10.1016/j.lithos.2014.06.020